RSC Advances

PAPER

View Article Online
View Journal | View Issue

Cite this: *RSC Adv.*, 2015, **5**, 21249

Exploration of a library of triazolothiadiazole and triazolothiadiazine compounds as a highly potent and selective family of cholinesterase and monoamine oxidase inhibitors: design, synthesis, X-ray diffraction analysis and molecular docking studies†

Imtiaz Khan,‡[a] Syeda Mahwish Bakht,[b] Aliya Ibrar,[a] Saba Abbas,[b] Shahid Hameed,*[a] Jonathan M. White,[c] Usman Ali Rana,[d] Sumera Zaib,[b] Mohammad Shahid[e] and Jamshed Iqbal*[b]

Received 15th January 2015
Accepted 12th February 2015

DOI: 10.1039/c5ra00906e

www.rsc.org/advances

There is a high demand for the collection of small organic molecules (especially *N*-heterocycles) with diversity and complexity in the process of drug discovery. This need for privileged scaffolds in medicinal research gives an impetus for the development of nitrogen-containing compounds which are widely encountered in natural products, drugs and pharmaceutically active compounds. In this context, a diverse library of new triazolothiadiazole (**4a–l**) and triazolothiadiazine (**5a–p**) compounds was designed, synthesized and evaluated as potent and selective inhibitors of *electric eel* acetylcholinesterase (EeAChE) and horse serum butyrylcholinesterase (hBChE) by Ellman's method using neostigmine and donepezil as standard inhibitors. Among the screened triazolothiadiazoles, **4j** emerged as a lead candidate showing the highest inhibition with an outstanding IC_{50} value of 0.117 ± 0.007 μM against AChE, which is ~139-fold greater inhibitory efficacy as compared to neostigmine, whereas **4k** displayed ~506-fold strong inhibition with IC_{50} of 0.056 ± 0.001 μM against BChE. In the triazolothiadiazine series, **5j** and **5e** depicted a clear selectivity towards EeAChE with IC_{50} values of 0.065 ± 0.005 and 0.075 ± 0.001 μM, respectively, which are ~250- and ~218-fold stronger inhibition as compared to neostigmine (IC_{50} = 16.3 ± 1.12 μM). In addition, the synthesized compounds were also tested for their monoamine oxidase (MAO-A and MAO-B) inhibition, where **4a** from the triazolothiadiazole series delivered the highest potency against MAO-A with an IC_{50} value of 0.11 ± 0.005 μM which is ~33-fold higher inhibition as compared to the standard inhibitor, clorgyline (IC_{50} = 3.64 ± 0.012 μM), whereas compound **5c** from the triazolothiadiazine series turned out to be a lead inhibitor with an IC_{50} value of 0.011 ± 0.001 μM which is ~330-fold stronger inhibition. Moreover, compounds **4b** (triazolothiadiazole series) and **5o** (triazolothiadiazine series) were identified as lead inhibitors against MAO-B. Molecular modelling studies were performed against human AChE and BChE to observe the binding site interactions of these compounds.

Introduction

Alzheimer's disease (AD) is a chronic, progressive, neurodegenerative disease[1,2] and it currently afflicts 24 million people worldwide.[1–3] It is the most common cause of senile dementia and is characterized by loss of both short term and long term memory due to neuronal loss, disorientation, difficulty in speaking or writing, loss of reasoning skills, and delusions,

[a]*Department of Chemistry, Quaid-i-Azam University, Islamabad-45320, Pakistan. E-mail: shameed@qau.edu.pk; Fax: +92-51-90642241; Tel: +92-51-90642133*

[b]*Centre for Advanced Drug Research, COMSATS Institute of Information Technology, Abbottabad-22060, Pakistan. E-mail: drjamshed@ciit.net.pk; Fax: +92-992-383441; Tel: +92-992-383591; +92-992-383596*

[c]*School of Chemistry and Bio-21 Institute, University of Melbourne, Parkville-3052, Australia*

[d]*Sustainable Energy Technologies (SET) Center, College of Engineering, King Saud University, PO-Box 800, Riyadh 11421, Saudi Arabia*

[e]*German Center for Neurodegenerative Diseases (DZNE), Germany*

† Electronic supplementary information (ESI) available. CCDC 1033196 and 1033197. For ESI and crystallographic data in CIF or other electronic format see DOI: 10.1039/c5ra00906e

‡ Present address: School of Chemistry, University of Nottingham, University Park, Nottingham, NG7 2RD, UK.

among other symptoms.[4] A multitude of features, including metal ion dyshomeostasis and disruption of both lipid production and membrane structure, have been implicated in AD onset and progression.[3] Recent research has suggested that some of these characteristics could be intertwined with other facets (*i.e.*, protein aggregation) of the disease.[2,3]

Two important enzymes from the group of serine hydrolases, acetylcholinesterase (AChE, EC 3.1.1.7) and butyrylcholinesterase (BChE, EC 3.1.1.8; also known as pseudocholinesterase), are usually defined as cholinesterases (ChEs). Structurally, these serine hydrolases belong to the class of proteins known as the esterase/lipase family within the α/β-hydrolase fold superfamily.[5] They differ in kinetics and substrate selectivity[6] and the major role of AChE is to catalyze the hydrolysis of acetylcholine (ACh) in cholinergic synapses, whereas the function of BChE is less clearly defined because it can hydrolyze ACh as well as other esters.[7,8] One of the major therapeutic strategies adopted for primarily symptomatic AD is based on the cholinergic hypothesis targeting cholinesterase enzymes (acetyl- and butyrylcholinesterase).[9] Inhibition of the hydrolysis of acetylcholine by blocking its metabolic enzyme acetylcholinesterase (AChE) increases the ACh concentration in cholinergic synapses and can subsequently affect a number of pathogenic processes and thereby provides a possible symptomatic treatment option for AD. On the other hand, butyrylcholinesterase (BChE) has recently been considered as a potential target because it also plays an important role in regulating ACh level.[10] ChE inhibitors (ChEIs) are used in the treatment of various neuromuscular disorders and have provided the first generation of drugs for the treatment of Alzheimer's disease.[11] AChE inhibitors currently approved as drugs for the treatment of Alzheimer's disease are donepezil, rivastigmine, galanthamine and tacrine. In view of the limited number of AChE inhibitors currently available on the market for the treatment of AD, the search for new ChEIs is of great interest and ongoing worldwide.

Monoamine oxidase (MAO; EC 1.4.3.4) is an important target to be considered for the treatment of AD, as catalyzes the oxidative deamination of a variety of biogenic and xenobiotic amines, with the concomitant production of hydrogen peroxide.[12] Monoamine oxidase is a flavin adenine dinucleotide (FAD) containing enzyme, which is localized in the outer mitochondrial membranes of neuronal, glial, and other cells[13] particularly abundant in the liver and brain.[14] MAO exists as two isozymes: MAO-A and MAO-B, showing different substrate specificity, sensitivity to inhibitors, and amino acid sequences. MAO-A preferentially oxidizes norepinephrine and serotonine, and is selectively inhibited by clorgyline, while MAO-B preferentially deaminates β-phenylethylamine and is irreversibly inhibited by l-deprenyl.[15] Selective MAO-A inhibitors are used clinically as antidepressants and anxiolytics, while MAO-B inhibitors are used for reduction of the progression of Parkinson's disease and of symptoms associated with Alzheimer's disease. Earlier MAO-inhibitors introduced into clinical practice for the treatment of depression were abandoned due to adverse side effects, such as 'cheese effect' characterized by hypertensive crises.[16] For this reason, there is currently a need for compounds that are useful for enhancing cognitive function and for treating cognitive deterioration in AD, as well as compounds that can generally improve cognition in normal, diseased, and aging subjects,[16] and presently the research has been directed towards the synthesis of new potential agents with possible clinical practice.

Nitrogen-containing heterocyclic compounds are the most abundant and integral scaffolds that occur ubiquitously in a variety of synthetic drugs, bioactive natural products, pharmaceuticals and agrochemicals. Owing to their widespread applications, these skeletons have long been a subject of immense interest, and substantial efforts have been made to the development of synthetic strategies which could lead to the discovery of new bioactive compounds in medicinal chemistry.[17] Among them, conjugated heterocycles like triazolothiadiazoles and triazolothiadiazines are associated with a wide range of biological activities including antimicrobial,[18] antitumor,[19] antiviral,[20] anticancer,[21] CNS depressant,[22] anti-inflammatory, analgesic,[23] antioxidant,[24] anti-HIV and anti-kinesin Eg5 activity.[25] Numerous triazolothiadiazole derivatives have also revealed potent urease, phosphodiesterase and c-Met protein inhibitory potential.[26,27] We have recently demonstrated the utility of these hybrid structures incorporating hetero-aromatic substituent (pyridine) at 3-position of the main skeleton

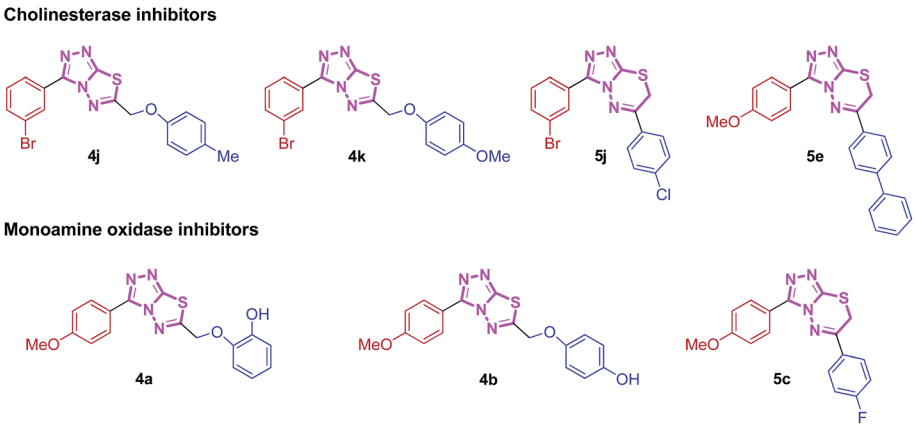

Fig. 1 Synthesized heteroaromatic structures with remarkable cholinesterase and monoamine oxidase inhibitory potential.

displaying potential cytotoxic, anti-cholinesterase, alkaline phosphatase and anti-leishmanial activities.[28,29] These *N*-bridgehead cholinesterase inhibiting lead structures were found to exhibit moderate activity and were used as a starting point for the development of highly potent and selective cholinesterase inhibitors. The cholinesterase inhibitory activities of these classes of compounds and their selectivity were dramatically improved by introducing a non-heteroaromatic substituents at 3-position. With this aim, we synthesized these hybrid fundamental templates with a variety of structural modifications and investigated SARs to find structures with high cholinesterase inhibitory potential. Additionally, the synthesized hybrids were also screened for their monoamine oxidase inhibition and were found to inhibit MAO-A selectively (Fig. 1). The results of this study are summarized in this paper.

Results and discussion

Chemistry

The target compounds were synthesized as outlined in Scheme 1. The key intermediate in the preparation of triazolothiadiazoles (**4a–l**) and triazolothiadiazines (**5a–p**) was 4-amino-1,2,4-triazole (**3a,b**) which in turn was prepared by a one-pot reaction of the corresponding benzoic acids (**1a,b**) with thiocarbohydrazide (**2**) at 190–200 °C.[30] While 4-amino-3-mercapto-1,2,4-triazoles (**3a,b**) may exist in thione–thiol tautomeric forms, in the present study, the thiol structure was dominated in the solid state. Routine spectroscopic methods including FTIR and ^{1}H NMR readily distinguished between these constitutional isomers.

The FTIR spectra of **3a** and **3b** showed absorption bands at 2554 and 2563 cm^{-1}, respectively, indicative of –SH group and no absorption band in the range 1300–1200 cm^{-1} attributable to the C=S group. The disappearance of the absorption bands for N–H in the range of 3400–3200 cm^{-1} also indicated the formation of thiol isomer. ^{1}H NMR spectra of 4-amino-triazoles (**3a,b**) exhibited resonances for –NH_2 protons as a singlet at 5.77 and 5.80 ppm (integrating two protons) and the –SH proton as a singlet at 13.83 and 14.03 ppm, respectively.

The reaction of corresponding 4-amino-1,2,4-triazole-3-thiol (**3a,b**) with aryloxy acids in the presence of phosphorous oxychloride delivered 1,2,4-triazolo[3,4-*b*][1,3,4]thiadiazoles (**4a–l**).[28,29] Their proton NMR spectra showed new peaks in the range of 5.80–8.53 ppm (integration for two protons) attributed to methylene protons, and lacked signals characteristic of –SH and –NH_2 protons, establishing that the –COOH group of the aryloxy acids reacted with –SH and –NH_2 groups of the intermediate **3a,b** to afford the corresponding conjugated products in efficient yields. Structural variations included electron-donating (–OH, –OMe, –Me) as well as electron-withdrawing (–F) substituents on the aryloxy ring attached to C-6 of triazolothiadiazole skeleton in addition to those present on aryl ring of benzoic acid attached to C-3 of the conjugated core.

Moreover, 1,2,4-triazolo[3,4-*b*][1,3,4]thiadiazines (**5a–p**) were prepared through the reaction of corresponding 4-amino-1,2,4-triazole-3-thiol (**3a,b**) with substituted phenacyl bromides in absolute ethanol under reflux.[28,29] Their proton ^{1}H NMR spectra showed that the signals due to –SH and –NH_2 protons had disappeared, and a new signal appeared at 4.58–4.40 ppm (integration for two protons) attributed to the methylene protons. This confirmed that the intermediate (**3a,b**) underwent ring closure to give the 1,2,4-triazolo[3,4-*b*]-[1,3,4]thiadiazines in good yields. The generality of this method is validated by using a diverse range of substituents (electron-rich and electron-deficient) on the aryl ring affording corresponding hybrid products in high yields. The cyclocondensation reaction also proceeds efficiently when α-bromo ketones with bulky biphenyl and naphthyl groups were used as coupling partners affording desired products in good yields. Furthermore, purity of the synthesized compounds was ascertained by elemental analysis.

X-ray crystallography

For a full structural elucidation, compounds **4i** and **5e** were confirmed by X-ray diffraction analysis. The crystal and

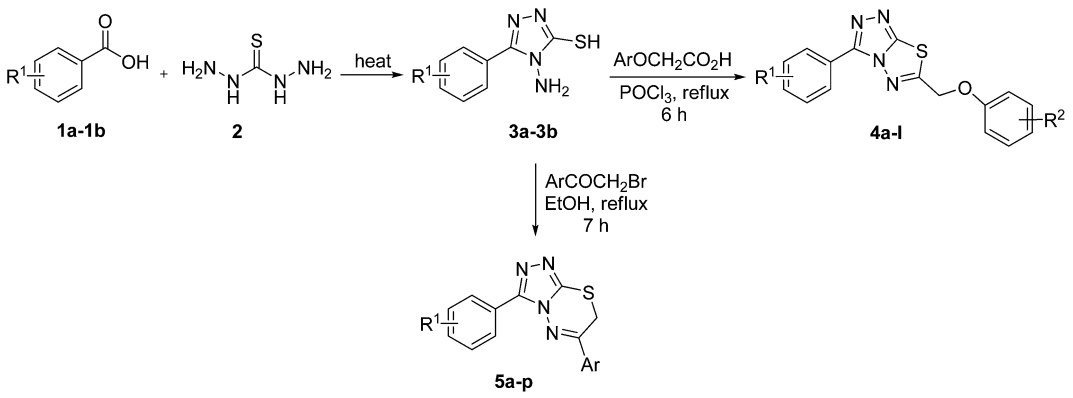

Scheme 1 Synthesis of triazolothiadiazoles (**4a–l**)and triazolothiadiazines (**5a–p**).

Table 1 Crystal data and structure refinement for **4i** and **5e**

Structural parameters	Compound **4i**	Compound **5e**
Empirical formula	$C_{17}H_{13}BrN_4OS$	$C_{23}H_{18}N_4OS$
Formula weight	401.28	398.47
Temperature (K)	130(2)	130(21)
Wavelength (Å)	0.7107	0.7107
Crystal system	Triclinic	Monoclinic
Space group	$P\bar{1}$	$P21/c$
Unit cell dimensions (Å)	$a = 7.5733(3)$, $\alpha = 105.441(5)^\circ$ $b = 10.0581(7)$, $\beta = 102.930(4)^\circ$ $c = 11.2828(6)$, $\gamma = 91.660(4)^\circ$	$a = 13.0300(3)$, $\alpha = 90^\circ$ $b = 17.3539(4)$, $\beta = 98.990(2)^\circ$ $c = 8.6142(2)$, $\gamma = 90^\circ$
Volume (Å^3)	803.82(8)	803.82(8)
Z	2	4
Density (calculated) (mg m^{-3})	1.584	1.376
Absorption coefficient (mm^{-1})	0.285	0.191
$F(000)$	404	832
Crystal size (mm^3)	0.59 × 0.39 × 0.18	0.35 × 0.2 × 0.15
Theta range for data collection (°)	2.973 to 29.121	2.903 to 29.188
Index ranges	$-9 \le h \le 10$, $-13 \le k \le 13$, $-14 \le l \le 12$	$-15 \le h \le 17$, $-23 \le k \le 20$, $-11 \le l \le 11$
Reflections collected	6521	11 392
Independent reflections	3736 [R(int) = 0.0331]	4578 [R(int) = 0.0382]
Completeness to theta = 25.242° (%)	99.7	99.8
Absorption correction	Gaussian	Semi-empirical from equivalents
Max. and min. transmission	0.639 and 0.328	1.00000 and 0.86346
Refinement method	Full-matrix least-squares on F^2	Full-matrix least-squares on F^2
Data/restraints/parameters	3736/0/218	4578/0/263
Goodness-of-fit on F^2	1.028	1.053
Final R indices [$I > 2\sigma(I)$]	$R_1 = 0.0349$, w$R_2 = 0.0729$	$R_1 = 0.0505$, w$R_2 = 0.1156$
R Indices (all data)	$R_1 = 0.0448$, w$R_2 = 0.0776$	$R_1 = 0.0736$, w$R_2 = 0.1343$
Largest diff. peak and hole (e Å^{-3})	0.472 and −0.512	0.316 and −0.400

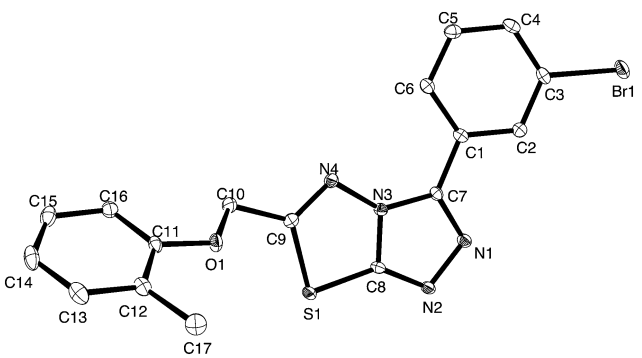

Fig. 2 Thermal ellipsoid plot for **4i**, ellipsoids are at the 30% probability level.

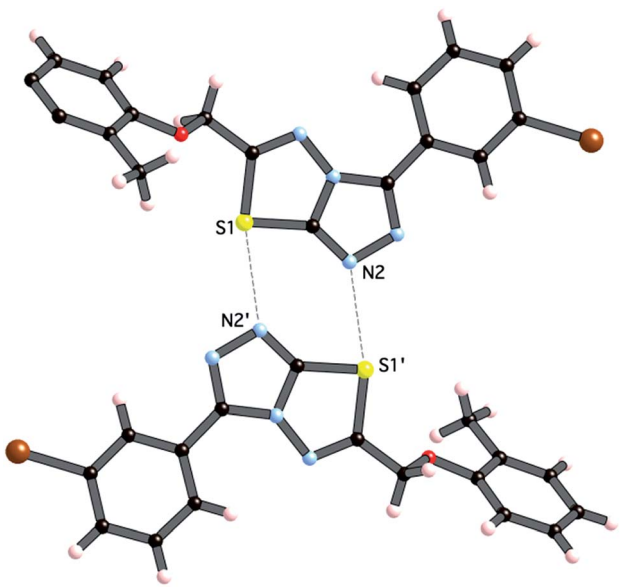

Fig. 3 Interaction between [1,2,4]triazolothiadiazole rings. Atoms labeled with a (′) are related by the symmetry operation (−x, −y, 1 − z).

instrumental parameters used in the unit cell determination, the data collection, and structure refinement parameters are presented in Table 1.

Compound 4i. A thermal ellipsoid plot for the [1,2,4]triazolo[3,4-*b*][1,3,4]thiadiazole (**4i**) is presented in Fig. 2. The bond distances within the [1,2,4]triazolo[3,4-*b*][1,3,4]thiadiazole ring system are in agreement with the mean values for the corresponding distances from 49 structures in the Cambridge Crystallographic Database (CSD) containing this moiety.[31] The bromophenyl substituent is essentially coplanar with the [1,2,4]triazolo[3,4-*b*][1,3,4]thiadiazole ring (C2–C1–C7–N3 dihedral angle = −174.0(2)°) and the RMS deviation of atoms from the plane defined by C1–C9, N1–N4, S1 = 0.077. The phenoxymethylene substituent is twisted from coplanarity with the triazolothiadiazole ring (dihedral angle S1–C9–C10–O1 = 55.8(2)°) while the conformation about the C11–O1 bond

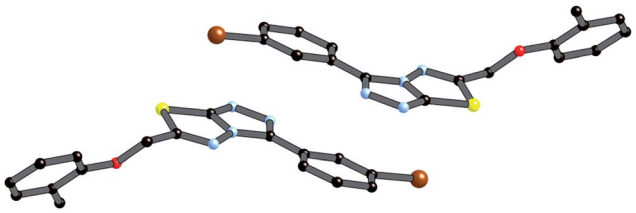

Fig. 4 π-stacking between centrosymmetrically related pair of the **4i** (symmetry operation is (−*x*, 1 − *y*, 1 − *z*).

(dihedral angle C10–O1–C11–C16 = −2.4(3)°) allows for conjugation of the oxygen p-type lone pair with the aromatic ring.

Crystals of **4i** are densely packed as a result a number of strong intermolecular interactions. The most important interactions are summarized in Fig. 3–5. The first of these is a strong complementary interaction between a pair of triazolothiadiazole rings related by a centre of inversion. The S1···N2 distance is 2.795(2) Å, which is 0.555 Å shorter than the sum of the van der Waals radii for nitrogen and sulfur. The N2′···S1–C9 angle which is 163.9(2)° suggests that this may be an example of a 'sigma-hole' type interaction between the nitrogen lone pair and the sulfur atom. A search of the CSD for structures containing the triazolothiadiazole ring system, revealed no contacts between the S atom and N donors in the crystal which were significantly shorter than 3.0 Å, therefore this structure provides the shortest example of a N···S interaction yet observed in these types of compounds.[32]

The crystal packing of **4i** is also stabilized by π-stacking interactions between pairs of the planar aryl-substituted triazolothiadiazole moieties. The distance between the mean planes of aryl-triazolothiadiazole is 3.342(2) Å while the centroid–centroid distance is 4.124 Å.

The third strong interaction evident in the packing of **4i** is a complementary C–H···π interaction between centrosymmetrically related pairs of phenoxymethylene moieties. The distance between H10A and the mean plane defined by atoms C11–C16 is 2.753(2) Å while the distance of H10A to the centroid of this ring is 2.820 Å.

A partial packing diagram indicating all these interactions is presented in Fig. 6.

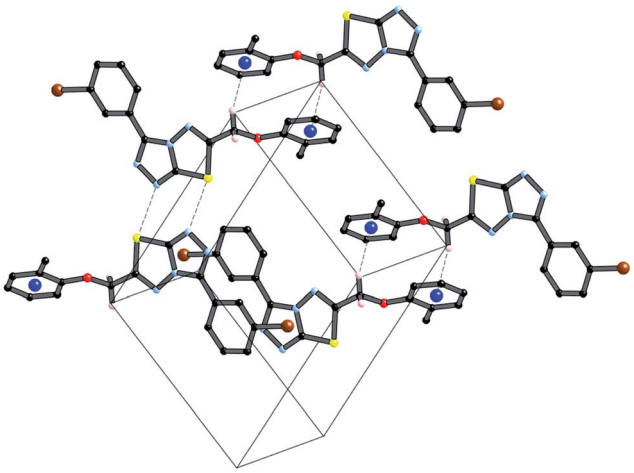

Fig. 6 Partial packing diagram illustrating the N···S sigma–hole interaction and the π–π and C–H···π interactions in crystals of **4i**.

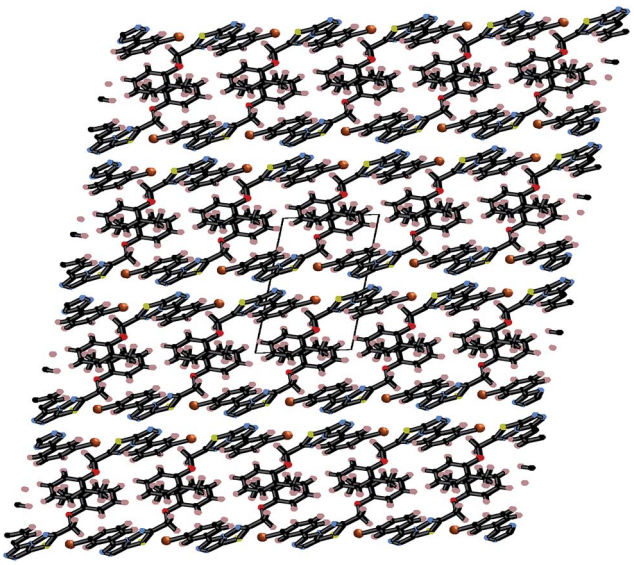

Fig. 7 Packing diagram of **4i** in the *xz* plane stabilized by π···π interactions.

These three strong interactions, which extend in all 3-dimensions in the crystal (Fig. 7 and 8), result in a densely packed crystal which has a high crystal density of 1.658 g cm^{-3}.

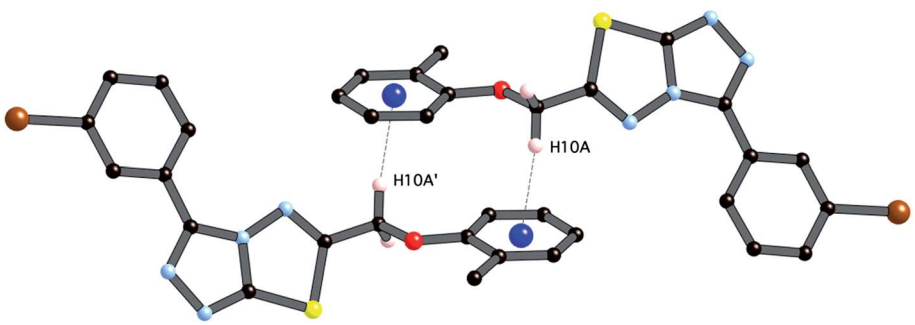

Fig. 5 C–H···π interaction between centrosymmetrically related pairs of **4i**, symmetry operator (1 − *x*, −*y*, −*z*).

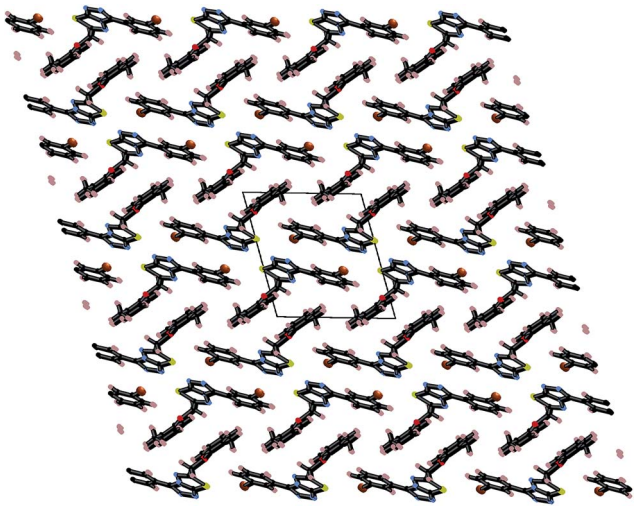

Fig. 8 Packing diagram of **4i** in the *yz* plane stabilized by both N···S sigma–hole interactions and C–H···π interactions.

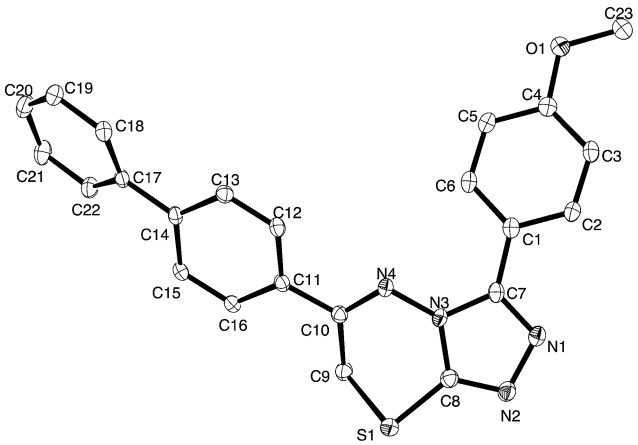

Fig. 9 Thermal ellipsoid plot for **5e**. Ellipsoids are at the 30% probability level.

Compound 5e. A thermal ellipsoid plot for 7*H*-[1,2,4]triazolo[3,4-*b*][1,3,4]thiadiazine (**5e**) is presented in Fig. 9. The bond distances within the 7*H*-[1,2,4]triazolo[3,4-*b*][1,3,4]thiadiazine ring system are closely similar to the mean bond distances obtained from 61 structures containing this ring system in the CSD. The methoxyphenyl substituent is essentially coplanar to the triazole ring (C2–C1–C7–N1 dihedral angle = −5.0(2)°) while the first biphenyl ring is close to coplanar with the C=N moiety in the thiadiazine ring (dihedral angles C16–C11–C10–C9 = −3.2(2)° and C16–C11–C10–N4 = 172.5(2)°, this conformation, which allows for conjugation between these two groups occurs at the cost of a close contact between hydrogen atoms attached to C16 and C9 (H16···H9b 1.94 Å). The biphenyl rings are twisted from coplanarity (C18–C17–C14–C13 dihedral angle = −26.5(2)°). The methoxyl substituent is near coplanar with the aromatic ring (dihedral angle C23–O1–C4–C3 = 10.5(2)°) this conformation allows for extensive delocalization of the oxygen lone-pair onto the ring through to the electron-deficient triazolothiadiazine moiety.

In contrast to compound **4i**, there are only relatively weak intermolecular interactions between molecules of **5e** in the crystal. The shortest interactions are between hydrogen atoms H15 and H16 and the nitrogen atoms N1 and N2 respectively (distances N1···h16 and N2···H15 are 2.68 and 2.46 Å, respectively (Fig. 10). Consistent with the relatively weak intermolecular contacts in the structure of **5e**, the crystal density 1.376 g cm^{-3} is significantly less than **4i**.

Pharmacological studies

Cholinesterase inhibition. The newly synthesized triazolothiadiazoles (**4a–l**) and triazolothiadiazines (**5a–p**) were assayed for inhibition against EeAChE and hBChE by Ellman's method[33] at micromolar level using neostigmine and donepezil as standard inhibitors. Their IC_{50} values for AChE are 16.3 ± 1.12 μM and 0.02 ± 0.003 μM, respectively. Whereas for BChE, neostigmine and donepezil showed IC_{50} value of 28.3 ± 2.06 and 7.23 ± 0.12 μM, respectively. The preliminary results revealed that the synthesized hybrid compounds exhibited remarkable cholinesterase inhibition which is many folds higher as compared to standard drugs. The results of this study are summarized in Tables 2 and 3.

Structure–activity relationship. On the basis of cholinesterase inhibitory activity results obtained for the prepared conjugated hybrid structures, we have used a three-zone approach to analyze the results and to guide our initial round of medicinal chemistry structure–activity relationship studies (Fig. 11 and 12). In particular, zone 2, the core heteroaromatic scaffold has found to be non-influential on the activity results. The zone 3 possessed a broad variation of substituents (electron-rich and electron-deficient) on the aryl ring and in certain cases aryl ring itself. The investigation of these exclusive modifications combined with zone 1 least alterations indicated a profound effect on the generation of lead structures with improved and selective inhibitory activity.

From the activity results presented in Table 2, it is evident that most of the hybrid compounds were significantly active for both AChE and BChE enzymes with more selectivity towards AChE. The variation of the substituents at aromatic rings (zone 1 and 3) significantly affected cholinesterase inhibitory potency and the selectivity as well. Remarkably, the behavior of these compounds is more selective for AChE than BChE inhibition having electron-rich (–OMe) group on phenyl ring attached at 3-position of conjugated skeleton. All the synthesized compounds (**4a–l**) were found to be significantly more potent against AChE than the standard drugs used. Among them, **4j** was the lead candidate showing highest inhibition with IC_{50} value of 0.117 ± 0.007 μM, which is ∼139-fold stronger inhibition as compared to neostigmine. This compound possessed a bromo substituent at the meta-position of the phenyl ring (zone 1) attached at 3-position along with a 4-methyl substituent at the *para*-position of the aromatic ring (zone 3) attached at 6-position of triazolothiadiazole core. The same compound showed nearly 50% inhibition against BChE demonstrating the

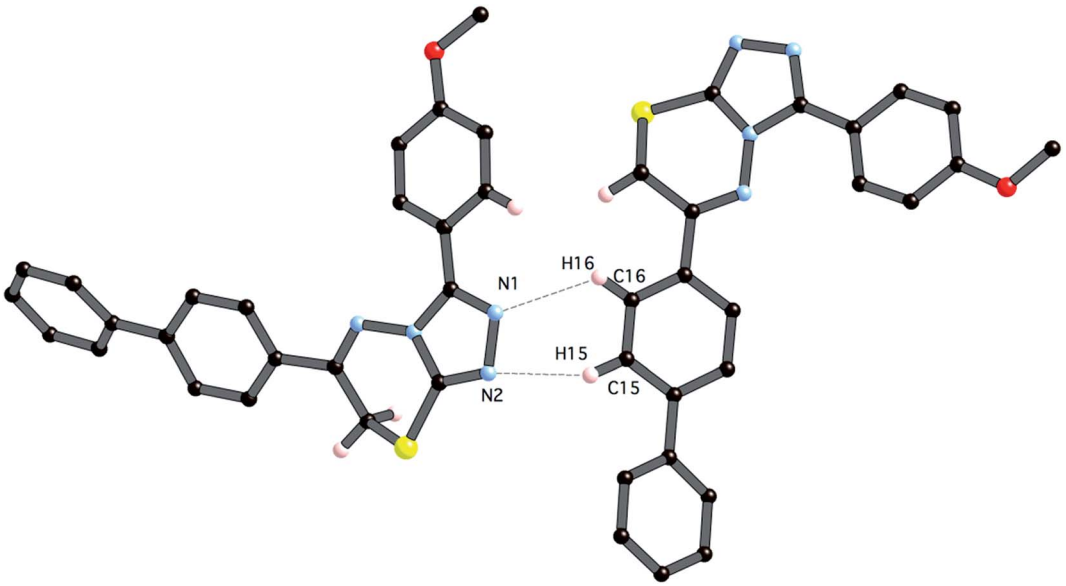

Fig. 10 Close intermolecular contacts between molecules of **5e** (symmetry code $x, y - 0.5, 0.5 + z$).

Table 2 AChE and BChE inhibition by newly synthesized triazolothiadiazoles (**4a–l**)[a]

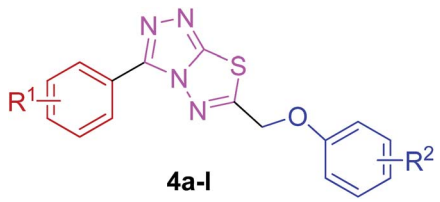

4a-l

Entry	R^1	R^2	AChE $IC_{50} \pm$ SEM (μM)	BChE $IC_{50} \pm$ SEM (μM)
4a	4-OMe	2-OH	0.282 ± 0.017	4.287 ± 0.023
4b	4-OMe	4-OH	0.538 ± 0.046	0.478 ± 0.011
4c	4-OMe	2-Me	3.302 ± 0.142	4.987 ± 0.028
4d	4-OMe	4-Me	0.564 ± 0.016	0.184 ± 0.007
4e	4-OMe	4-OMe	0.245 ± 0.024	1.142 ± 0.013
4f	4-OMe	4-F	0.272 ± 0.018	0.175 ± 0.003
4g	3-Br	2-OH	0.213 ± 0.008	2.235 ± 0.014
4h	3-Br	4-OH	0.152 ± 0.004	2.354 ± 0.051
4i	3-Br	2-Me	0.311 ± 0.013	2.012 ± 0.018
4j	3-Br	4-Me	0.117 ± 0.007	1.971 ± 0.032
4k	3-Br	4-OMe	0.159 ± 0.014	0.056 ± 0.001
4l	3-Br	4-F	0.227 ± 0.013	0.168 ± 0.003
Neostigmine	—	—	16.3 ± 1.12	28.3 ± 2.06
Donepezil	—	—	0.02 ± 0.003	7.23 ± 0.12

[a] IC_{50} = concentration of inhibitor required for half-maximal enzyme inhibition and are reported as means of two independent experiments, each performed in triplicate (SEM, standard error of the mean).

Table 3 AChE and BChE inhibition by newly synthesized triazolothiadiazines (**5a–p**)[a]

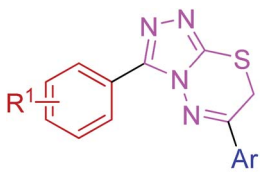

5a-p

Entry	R^1	Ar	AChE $IC_{50} \pm$ SEM (μM)	BChE $IC_{50} \pm$ SEM (μM)
5a	4-OMe	4-OMe-Ph	0.870 ± 0.051	0.176 ± 0.013
5b	4-OMe	4-Cl-Ph	1.09 ± 0.072	0.362 ± 0.015
5c	4-OMe	4-F-Ph	0.365 ± 0.013	3.422 ± 0.008
5d	4-OMe	4-Me-Ph	0.220 ± 0.005	0.066 ± 0.021
5e	4-OMe	Biphenyl	0.075 ± 0.001	3.936 ± 0.041
5f	4-OMe	Naphthyl	0.496 ± 0.016	3.174 ± 0.007
5g	4-OMe	4-NO_2-Ph	0.205 ± 0.013	2.382 ± 0.004
5h	4-OMe	3,4-Cl_2-Ph	0.301 ± 0.011	2.547 ± 0.016
5i	3-Br	4-OMe-Ph	0.747 ± 0.042	0.748 ± 0.004
5j	3-Br	4-Cl-Ph	0.065 ± 0.005	1.445 ± 0.0124
5k	3-Br	4-F-Ph	0.259 ± 0.031	1.384 ± 0.016
5l	3-Br	4-Me-Ph	0.950 ± 0.085	3.981 ± 0.0015
5m	3-Br	Biphenyl	1.303 ± 0.12	0.480 ± 0.028
5n	3-Br	Naphthyl	1.066 ± 0.76	0.343 ± 0.012
5o	3-Br	4-NO_2-Ph	0.854 ± 0.93	0.780 ± 0.062
5p	3-Br	3,4-Cl_2-Ph	0.248 ± 0.021	1.07 ± 0.084
Neostigmine	—	—	16.3 ± 1.12	28.3 ± 2.06
Donepezil	—	—	0.02 ± 0.003	7.23 ± 0.12

[a] IC_{50} = concentration of inhibitor required for half-maximal enzyme inhibition and are reported as means of two independent experiments, each performed in triplicate (SEM, standard error of the mean).

selective inhibitory potential towards AChE. Replacement of the zone 1 meta-bromo group with a *para*-methoxy substituent also afforded good inhibition against AChE (compound **4d**; IC_{50} = 0.564 ± 0.016 μM; ~29-fold strong inhibition) in addition to the

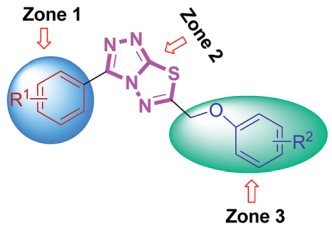

Fig. 11 The synthesized triazolothiadiazole structures (**4a–l**) investigated herein.

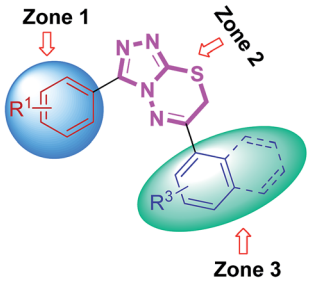

Fig. 12 The synthesized triazolothiadiazine structures (**5a–p**) investigated herein.

Table 4 Monoamine oxidase inhibition by triazolothiadiazoles (**4a–l**)[a]

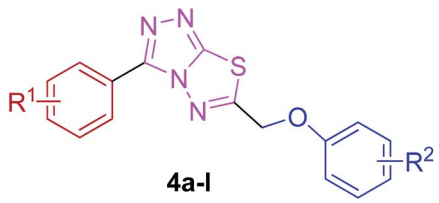

4a-l

			MAO-A	MAO-B
Entry	R^1	R^2	IC_{50} ± SEM (μM)	
4a	4-OMe	2-OH	0.11 ± 0.005	14.24 ± 1.03
4b	4-OMe	4-OH	0.25 ± 0.003	0.03 ± 0.001
4c	4-OMe	2-Me	0.11 ± 0.007	0.33 ± 0.009
4d	4-OMe	4-Me	0.24 ± 0.008	4.36 ± 0.21
4e	4-OMe	4-OMe	1.85 ± 0.005	1.02 ± 0.003
4f	4-OMe	4-F	4.77 ± 0.13	0.606 ± 0.014
4g	3-Br	2-OH	14.65 ± 0.09	21.73 ± 0.027
4h	3-Br	4-OH	7.42 ± 0.2	25.31 ± 0.02
4i	3-Br	2-Me	1.23 ± 0.06	1.73 ± 0.09
4j	3-Br	4-Me	1.23 ± 0.003	1.42 ± 0.005
4k	3-Br	4-OMe	2.89 ± 0.007	2.97 ± 0.009
4l	3-Br	4-F	6.90 ± 0.34	0.87 ± 0.006
Clorgyline	—	—	3.64 ± 0.012	—
Deprenyl	—	—	—	0.007 ± 0.001

[a] IC_{50} = concentration of inhibitor required for half-maximal enzyme inhibition and are reported as means of two independent experiments, each performed in triplicate (SEM, standard error of the mean).

~154-fold higher potency against BChE as compared to **4j**. Among the same set of derivatives, the substituent electronic effect at various positions in zone 3 modulated the ChE

Table 5 Monoamine oxidase inhibition by triazolothiadiazines (**5a–p**)[a]

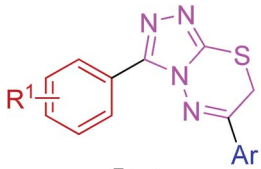

5a-p

			MAO-A	MAO-B
Entry	R^1	Ar	IC_{50} ± SEM (μM)	
5a	4-OMe	4-OMe-Ph	0.22 ± 0.004	0.18 ± 0.002
5b	4-OMe	4-Cl-Ph	0.92 ± 0.007	3.66 ± 0.003
5c	4-OMe	4-F-Ph	0.011 ± 0.001	5.92 ± 0.005
5d	4-OMe	4-Me-Ph	5.64 ± 0.030	15.21 ± 0.170
5e	4-OMe	Biphenyl	0.09 ± 0.006	28.59 ± 2.070
5f	4-OMe	Naphthyl	1.23 ± 0.009	6.03 ± 0.370
5g	4-OMe	4-NO_2-Ph	0.82 ± 0.005	34.82 ± 0.041
5h	4-OMe	3,4-Cl_2-Ph	16.5 ± 1.070	42.78 ± 0.037
5i	3-Br	4-OMe-Ph	2.08 ± 0.010	40.19 ± 0.025
5j	3-Br	4-Cl-Ph	1.69 ± 0.004	32.09 ± 0.17
5k	3-Br	4-F-Ph	3.92 ± 0.620	0.32 ± 0.017
5l	3-Br	4-Me-Ph	2.17 ± 0.130	3.68 ± 0.170
5m	3-Br	Biphenyl	1.21 ± 0.004	3.86 ± 0.050
5n	3-Br	Naphthyl	3.51 ± 0.060	18.7 ± 0.100
5o	3-Br	4-NO_2-Ph	13.94 ± 0.900	0.08 ± 0.0003
5p	3-Br	3,4-Cl_2-Ph	0.02 ± 0.0005	0.67 ± 0.009
Clorgyline	—	—	3.64 ± 0.012	—
Deprenyl	—	—	—	0.007 ± 0.001

[a] IC_{50} = concentration of inhibitor required for half-maximal enzyme inhibition and are reported as means of two independent experiments, each performed in triplicate (SEM, standard error of the mean).

inhibition as shown by compounds **4g–i**. In general, all the synthesized triazolothiadiazole compounds were emerged as efficient inhibitors of AChE whereas compounds **4b**, **4e**, **4f**, **4k**, and **4l** were found as potent candidates for BChE inhibition. It was also found that the combination of electron-rich and electron-deficient substituents in zone 1 and 3 resulted in stronger and selective inhibitors of AChE as compared to BChE where this combination is underlined in selected examples.

The newly synthesized triazolothiadiazine hybrids were also evaluated *in vitro* as inhibitors of *electric eel* acetylcholinesterase (EeAChE) and horse serum butyrylcholinesterase (hBChE). The inhibitory activities of novel compounds were compared to those of neostigmine and donepezil. All of the novel target analogues proved to be very potent and selective inhibitors of cholinesterases displaying inhibition abilities in micromolar range. A careful insight and analysis of the data listed in Table 3 led to several eventual structure–activity relationships (SAR) using a similar three zone approach (Fig. 12).

Some interesting considerations can be made by comparing enzyme inhibition data (Table 3) for the two sets of products bearing the same substituent in the zone 3 but variable groups (electron-rich and electron-deficient) on phenyl ring in zone 1. The majority of tested hybrids in the first set of compounds

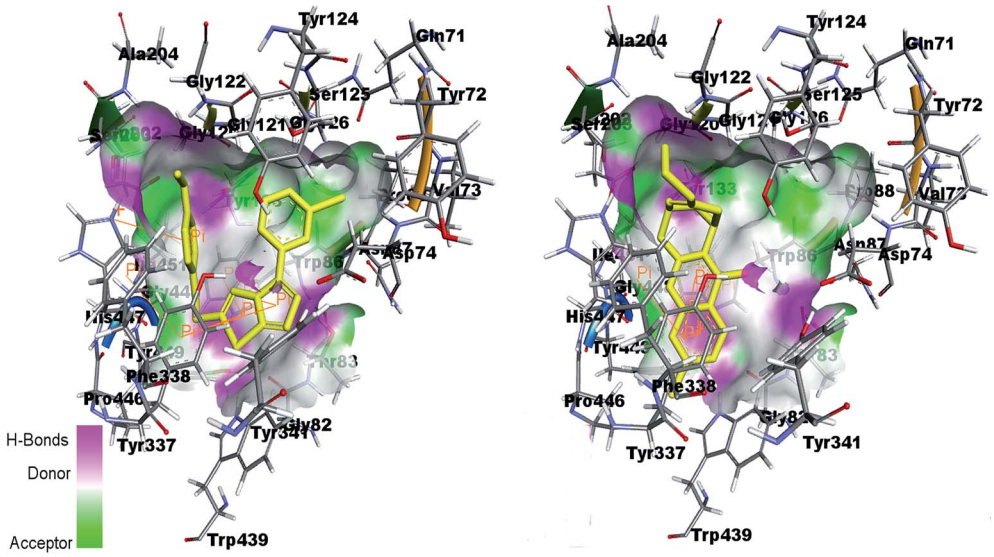

Fig. 13 Binding site interactions of amino acids inside the active pockets of AChE for reference ligand huprine W (right) and the potent compound **4k** (left).

bearing *para*-methoxy group in zone 1 depicted a clear selectivity towards EeAChE highlighting **5e** as the most potent AChE inhibitor in the series with IC_{50} value of 0.075 ± 0.001 μM which is ~218-fold stronger inhibition as compared to neostigmine (IC_{50} = 16.3 ± 1.12 μM). This compound incorporates bulky biphenyl ring in zone 3 in addition to *para*-methoxy group in zone 1. Similar results were also obtained when the biphenyl ring at C-6 is replaced with another sterically demanding naphthyl group (compound **5f**: IC_{50} = 0.496 ± 0.016 μM). The compounds incorporating electron-deficient substituents such as **5g** (4-NO_2) and **5h** (3,4-Cl_2) also revealed notable selective inhibition towards AChE with IC_{50} of 0.205 ± 0.013 μM (~79-fold stronger inhibition) and 0.301 ± 0.011 μM (~54-fold stronger inhibition), as compared to neostigmine. Within the first set of derivatives, compound **5d** was the lead candidate against BChE with IC_{50} value of 0.066 ± 0.021 μM (~427- and 109-fold stronger inhibition) as compared to neostigmine and donepezil, respectively. Other potent inhibitors of BChE are compounds **5a** and **5b** showing ~160- and 78-fold stronger inhibition (IC_{50} = 0.176 ± 0.013 and 0.362 ± 0.015 μM, respectively) as compared to standard drug neostigmine.

In the second set of compounds where a *meta*-bromo substituent is present on the aromatic ring (zone 1), **5j** emerged as a lead compound against AChE with IC_{50} value of 0.065 ± 0.005 μM showing ~250-fold higher potency as compared to neostigmine in addition to ~20-fold stronger inhibition against

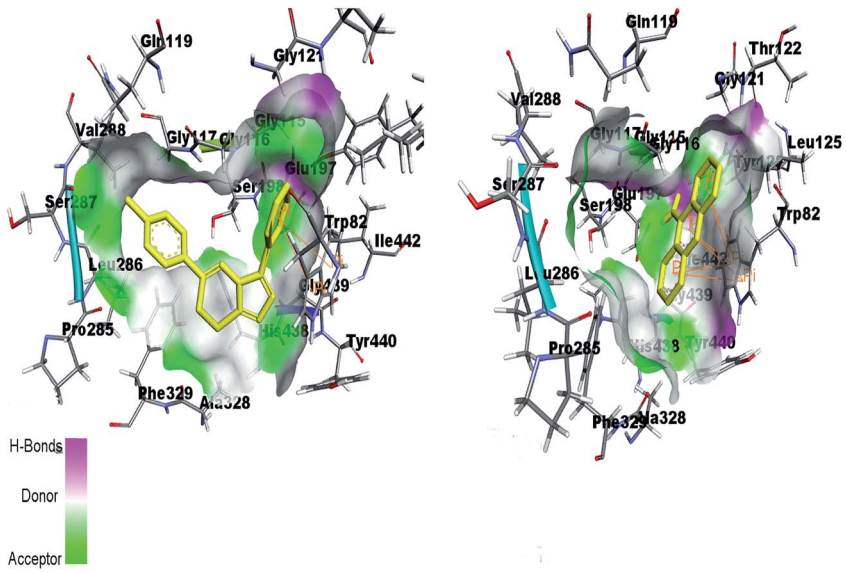

Fig. 14 Binding site interactions of amino acids inside the active pockets of BChE for reference ligand tacrine (right) and the potent compound **5d** (left).

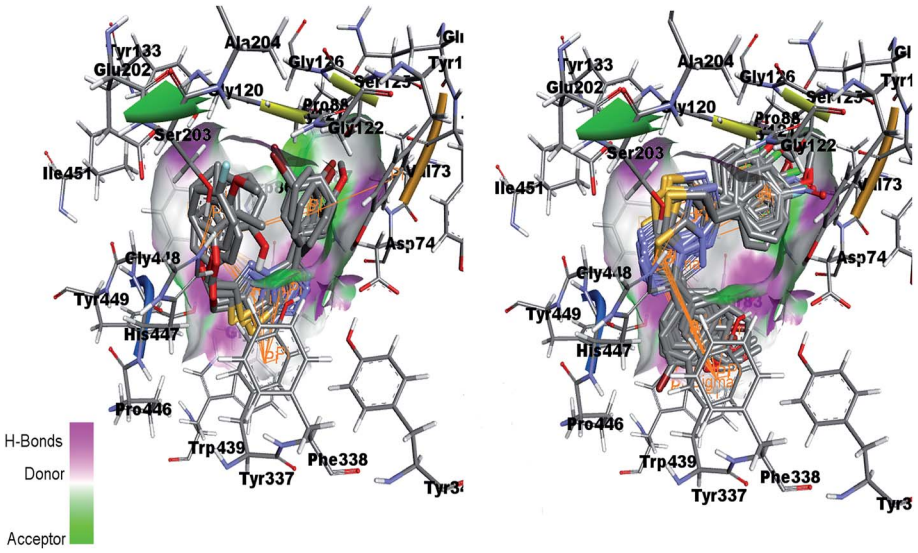

Fig. 15 Overlap of **4a**, **4i**, **4j**, **4k** and **4l** inside active site of AChE (left) and overlap of **5a**, **5b**, **5g**, **5h**, **5i**, **5j**, **5k**, **5l**, **5n**, **5o** and **5p** in the active pocket of AChE (right).

BChE (IC_{50} = 1.445 ± 0.0124 μM). This lead compound incorporates a combination of electron-withdrawing substituents (Br and Cl) on aryl ring in zone 1 and 3 at meta- and *para*-position, respectively. Similar results were acquired when another chloro substituent is introduced at 3-position (compound **5p**; IC_{50} = 0.248 ± 0.021 μM against AChE and IC_{50} = 1.07 ± 0.084 μM against BChE). The replacement of electronically poor substituents with sterically encumbered substituents like biphenyl and naphthyl in zone 3 (compounds **5m** and **5n**; IC_{50} = 1.303 ± 0.12 and IC_{50} = 1.066 ± 0.76 μM, respectively) produced excellent inhibitions of both AChE and BChE with more selectivity towards BChE. In general, most of the compounds were found as potent and selective inhibitors of cholinesterases and the results obtained clearly indicated the influence of electronic and steric properties of substituents on the cholinesterase inhibition as well as selectivity.

Monoamine oxidase inhibition. The inhibitory activity of monoamine oxidases A and B was measured *in vitro* by using a spectrophotometric method.[34] The percentage of MAO inhibition was determined for all the examined compounds and IC_{50} data were measured only for the evaluated compounds (Tables 4 and 5). Clorgyline and deprenyl were used as standard inhibitors with IC_{50} values of 3.64 ± 0.012 and 0.007 ± 0.001 μM, respectively.

At a first glance, the inhibition data reported in Table 4 indicated that most of the examined triazolothiadiazole compounds exhibited a very high and selective inhibition of MAO-A as compared to MAO-B. Among the synthesized

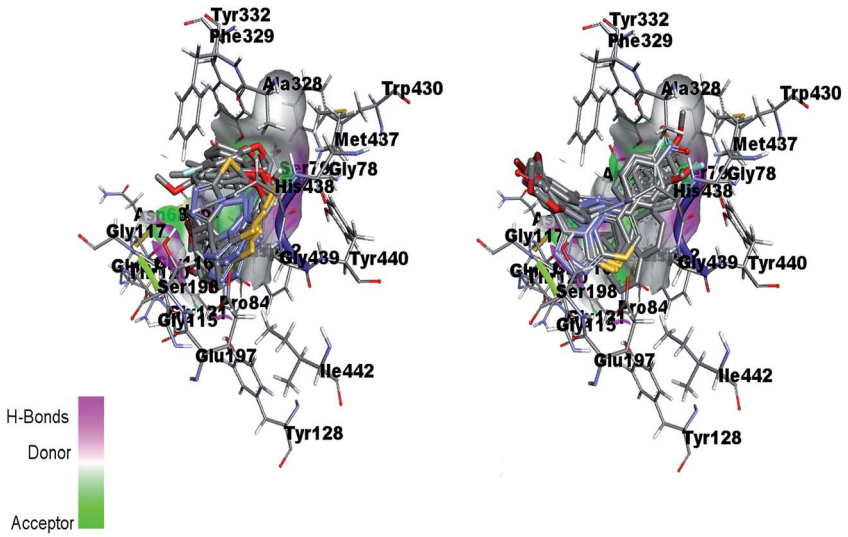

Fig. 16 Overlap of **4a**, **4c**, **4d**, **4e**, **4g**, **4i**, **4j** and **4l** inside active site pocket of BChE (left) and overlap of **5a**, **5b**, **5c**, **5f**, **5g**, **5i**, **5j**, **5k**, **5l**, **5n**, **5o** and **5p** in the active pocket of BChE (right).

Table 6 Docking scores for the triazolothiadiazoles (**4a–l**) screened against AChE and BChE

	AChE	BChE
Codes	Docking scores (kcal mol^{-1})	
4a	−9.59	−8.56
4b	−9.53	−9.38
4c	−10.03	−8.95
4d	−9.89	−8.37
4e	−9.88	−7.85
4f	−9.66	−8.25
4g	−10.01	−9.02
4h	−10.76	−9.05
4i	−10.33	−10.05
4j	−10.34	−9.36
4k	−10.64	−8.56
4l	−9.96	−9.83

Table 7 Docking scores for the triazolothiadiazines (**5a–p**) screened against AChE and BChE

	AChE	BChE
Codes	Docking scores (kcal mol^{-1})	
5a	−10.13	−9.16
5b	−10.21	−9.49
5c	−10.43	−8.65
5d	−10.85	−9.07
5e	−9.47	−6.91
5f	−11.92	−10.18
5g	−10.08	−8.31
5h	−10.15	−9.53
5i	−11.01	−9.86
5j	−11.02	−10.17
5k	−10.38	−9.48
5l	−10.86	−10.17
5m	−10.1	−8.11
5n	−11.77	−11.08
5o	−11.14	−9.45
5p	−11.16	−10.78

compounds, **4a** delivered highest potency against MAO-A with IC_{50} value of 0.11 ± 0.005 μM which is ~33-fold higher inhibition as compared to standard inhibitor, clorgyline (IC_{50} = 3.64 ± 0.012 μM). The previously mentioned SAR strategy was applied to explain the activity results (Fig. 11). According to that the most active analogue **4a** possesses electron-donating groups at the *para*- and *ortho*-position of both aryl rings in zone 1 and 3, respectively. The replacement of the 2-hydroxy group with another electron-rich (–Me) group produced similar results (compound **4c**; IC_{50} = 0.11 ± 0.007 μM, ~33-fold strong inhibition). The change of substitution position on the aryl ring in zone 3 had a positive influence on the inhibitory activity. Compounds **4d** and **4b** were also found to exhibit significant inhibitions with IC_{50} values of 0.24 ± 0.008 (15-fold strong inhibition) and 0.25 ± 0.003 μM (14-fold strong inhibition), respectively. Similarly, compounds obtained by replacing bromo group with methoxy group (**4i** and **4j**) also showed significant inhibition against MAO-A with IC_{50} values of 1.23 ± 0.06 and 1.23 ± 0.003 μM, respectively. The extent of this inhibition was found to be higher (~3-fold) as compared to the standard clorgyline. The introduction of electron-withdrawing (–F) group at *para*-position of phenyl ring attached to C-6 of heteroaromatic core led to reduced activity as compared to the clorgyline (compound **4f**; IC_{50} = 4.77 ± 0.13 μM). The combination of electron-deficient (–Br) group in zone 1 and electron-rich (–OH) group in zone 3 abolished the activity (compound **4g**; IC_{50} = 14.65 ± 0.09 μM).

On the other hand, the synthesized triazolothiadiazoles showed reduced activity against MAO-B as compared to the standard deprenyl (IC_{50} = 0.007 ± 0.001 μM). The most active MAO-B inhibitor was compound **4b** which showed an IC_{50} value of 0.03 ± 0.001 μM. This compound incorporates electron-rich functional groups at *para*-position of both aryl rings in zone 1 and 3. To sum up, MAO-A inhibitory potency of triazolothiadiazole compounds appeared to be mainly modulated by electronic effect which is clearly evidenced by the results presented herein whereas synthesized derivatives were inactive against MAO-B.

Similarly, all the synthesized triazolothiadiazine compounds were also evaluated for their ability to inhibit MAO-A and MAO-B. The corresponding IC_{50} values are shown in Table 5. The previously discussed SAR model (Fig. 12) was used to construct correlation between structural properties and biological activity results. Among the tested derivatives, compound **5c** turned to be a lead candidate with IC_{50} value of 0.011 ± 0.001 μM which is ~330-fold strong inhibition as compared to the standard inhibitor (clorgyline) used for comparison purpose. This compound incorporates a *para*-methoxy group at aromatic ring in zone 1 along with an electron-deficient (–F) functional group at aromatic ring in zone 3. The replacement of methoxy substituent with bromo group and introduction of two electron-withdrawing chloro substituents also produced similar results (compound **5p**; IC_{50} = 0.02 ± 0.0005 μM, ~182-fold strong inhibitory efficacy). Apart from electronic parameters, the steric effects were also found to contribute positively towards the inhibition of MAO-A. In this regard, compound **5e** exhibited strong inhibition with an IC_{50} value of 0.09 ± 0.006 μM which is 40-fold higher as compared to the standard inhibitor (clorgyline), whereas, the introduction of bulky naphthyl group led to the reduction in activity (IC_{50} = 1.23 ± 0.009 μM). But, still this inhibitory potential is 3-fold higher as compared to clorgyline. The synthesized structures with a combination of *para*-methoxy group and *para*-nitro or -chloro were also emerged as potent inhibitors of MAO-A (compound **5g**; IC_{50} = 0.82 ± 0.005 and 0.92 ± 0.007 μM; ~4.4- and ~4-fold stronger inhibition, respectively). On the other hand, prepared compounds were also tested for MAO-B inhibition but the activity profile was diminished for the screened derivatives. In the evaluated series, compound **5o** was found to demonstrate a highest inhibitory potency towards MAO-B with an IC_{50} value of 0.08 ± 0.0003 μM as compared to the standard, deprenyl (IC_{50} = 0.007 ± 0.001 μM). This compound incorporates a *meta*-bromo substituent on aromatic ring in zone 1 in addition to the highly polarizable

Table 8 *In silico* physicochemical properties of triazolothiadiazoles (**4a–l**) and triazolothiadiazines (**5a–p**)[a]

Codes	milog *P*	TPSA	n_{atoms}	MW	n_{ON}	n_{OHNH}	$n_{violations}$	n_{rotb}	volume
4a	3.026	81.787	25.0	354.391	7	1	0	5	293.812
4b	3.24	81.787	25.0	354.391	7	1	0	5	293.812
4c	4.12	61.559	25.0	352.419	6	0	0	5	302.355
4d	4.168	61.559	25.0	352.419	6	0	0	5	302.355
4e	3.776	70.793	26.0	368.418	7	0	0	6	311.34
4f	3.883	61.559	25.0	356.382	6	0	0	5	290.726
4g	3.754	72.553	24.0	403.261	6	1	0	4	286.152
4h	3.968	72.553	24.0	403.261	6	1	0	4	286.152
4i	4.848	52.325	24.0	401.289	5	0	0	4	294.695
4j	4.896	52.325	24.0	401.289	5	0	0	4	294.695
4k	4.504	61.559	25.0	417.288	6	0	0	5	303.68
4l	4.611	52.325	24.0	405.252	5	0	0	4	283.065
5a	3.95	61.55	25.0	352.419	6	0	0	4	302.355
5b	4.571	52.316	24.0	356.838	5	0	0	3	290.345
5c	4.057	52.316	24.0	340.383	5	0	0	3	281.741
5d	4.342	52.316	24.0	336.42	5	0	0	3	293.371
5e	5.688	52.316	29.0	398.491	5	0	1	4	348.218
5f	5.052	52.316	27.0	372.453	5	0	1	3	320.801
5g	3.852	98.14	26.0	367.39	8	0	0	4	300.144
5h	5.177	52.316	25.0	391.283	5	0	1	3	303.881
5i	4.702	52.316	24.0	401.289	5	0	0	3	294.695
5j	5.323	43.082	23.0	405.708	4	0	1	2	282.685
5k	4.809	43.082	23.0	389.253	4	0	0	2	274.081
5l	5.094	43.082	23.0	385.29	4	0	1	2	285.71
5m	6.441	43.082	28.0	447.361	4	0	1	3	340.558
5n	5.805	43.082	26.0	421.323	4	0	1	2	313.141
5o	4.604	88.906	25.0	416.26	7	0	0	3	292.483
5p	5.929	43.082	24.0	440.153	4	0	1	2	296.221

[a] milog *P* = octanol–water partition coefficient, TPSA = Topological Polar Surface Area, n_{atoms} = number of atoms, MW = molecular weight, n_{ON} = number of hydrogen acceptor, n_{OHNH} = number of hydrogen donor, $n_{violations}$ = violations from Lipinski's rule, n_{rotb} = number of rotatable bonds.

para-nitro group on phenyl ring in zone 3. In general, both electronic and steric factors were actively found to modulate the MAO inhibition and the presented derivatives (triazolothiadiazoles and triazolothiadiazines) are proved to be better and selective MAO-A inhibitors and these data are an important observation to follow up a rational design of more potent and selective inhibitors of monoamine oxidases (MAO).

Docking studies. The X-ray structures of human AChE (PDB ID: 4BDT) and BChE (PDB ID: 4BDS) were selected for the docking study because the available electric eel structures for AChE are of low crystallographic resolutions (>4 Å) and structures of equine BChE are not available at the moment. The active sites of AChE and BChE show a high degree of similarity despite the replacement of residues Pro446, Tyr124 and Phe297 in the active site of AChE by residues Met437, Gln119 and Val288 in BChE. In addition, residue Tyr337 in AChE is replaced by the smaller Ala328 in BChE.

Docking validation was carried out by re-docking the ligand extracted from the experimentally determined enzyme-ligand adduct. The docking method was able to reproduce the experimentally observed bound conformation of the co-crystallized ligand with rmsd <2 Å. By re-docking the crystallographic ligand huprine W in the active site of AChE, similar interactions were seen with the residues Tyr337, Trp86, Gly122, Ser203 as huprine W showed in the crystal structure of AChE. The ring system of both compound series adapts a comparable position to huprine W and it interacts with side chain atoms of several aromatic residues including Tyr337 and Trp86. Furthermore, residue Thr83 is found to be involved in hydrogen bonding with triazolothiadiazole and triazolothiadiazine ring of compounds. The phenyl rings having different substituents at both ends of the compounds are directed towards the hydrophobic pockets formed by the residues Gly121, Phe297 and Gly122. π–π stacking is also observed by most of the compounds in the active site.

Fig. 13 shows the interactions of amino acids in the active site of AChE by co-crystal ligand huprine W in the right side and potent compound **4k** in the left side. The figure shows that Trp86 and Tyr337 are involved in π-interaction with the ligand as well as compound **4k**. His447 is also showing π-interaction in the active pocket. It is therefore predicted that the docking of the compounds in the active site of enzyme showed the similar interactions as shown by co-crystal ligand.

By re-docking the crystallographic ligand tacrine in the active site of BChE, the most important residue involved in the active site is Try82 showing π–π interaction with tacrine. The triazolothiadiazole (**4a–l**) and triazolothiadiazine (**5a–p**) ring system adapts a comparable position to tacrine and almost all the docked compounds interact with non-polar Try82 and shows hydrophobic interactions. Fig. 14 shows the similar binding interactions by reference ligand and compound **5d**. Trp82 is involved in π-interaction as shown in figure.

Fig. 15 (left) showed the predicted conformations of compounds **4a**, **4i**, **4j**, **4k** and **4l** in the active site pocket of AChE. Similarly, Fig. 15 (right) represents the predicted conformations of compounds **5a**, **5b**, **5g**, **5h**, **5i**, **5j**, **5k**, **5l**, **5n**, **5o** and **5p** in the active site pocket of AChE. For the **4a–l** series of compounds, the central portion of triazolothiadiazole ring is directed towards the residues Gly82, Thr83, Tyr337 and Phe338 while the phenyl rings at the tails are directed towards the residues Trp86, Gly120, Gly121, Gly122, Asp74, Asn87, His447 and Gly448 and Gly82. In case of **5a–p**, the tails having phenyl rings bearing different substituents attached are directed towards the residues Trp439, Asp74, Val73 and Ser125. Whereas, the triazolothiadiazine ring present at center is directed into pocket and residues Gly121, Gly126, Leu130, Gly448, His447, Tyr449 and Ser203 are involved in the interactions.

Fig. 16 (left) showed the predicted conformations of compounds **4a**, **4c**, **4d**, **4e**, **4g**, **4i**, **4j** and **4l** in the active site pocket of BChE. Similarly, Fig. 16 (right) represented the predicted conformations of compounds **5a**, **5b**, **5c**, **5f**, **5g**, **5i**, **5j**, **5k**, **5l**, **5n**, **5o** and **5p** in the active site pocket of BChE. In case of BChE active pocket, the residues Ser79, Trp82, Asn83, Gly121 and Gly78 are involved in the interaction with the phenyl rings at tails in the **4a–l** series of compounds. Whereas, the central portion of triazolothiadiazole ring is directed towards the residues Gly115, Ser198, Gly439, Gly197 and Ala328. For **5a–p** series, the triazolothiadiazine ring present at centre is directed into pocket and residues Asp70, Try86, Gly116, Ser198 and Try449 are involved in the interactions and the tails having phenyl rings with different substituents are directed towards the residues Phe398, Ser198, Trp430, Ala328.

Our docking scores demonstrated that most of the compounds of both the series possessed similar binding modes with different docking scores as shown in Tables 6 and 7. Along with other studies, when compounds were evaluated for drug likeness and oral bioavailability, the results were in accordance with Lipinski's rule of five parameters (Table 8). The TPSA values showed that compounds in the form of drugs can be easily penetrable as all compounds showed polar surface area in the range of 43–99 $Å^2$. In general, for molecules to penetrate the blood–brain barrier and therefore to act as a receptor, an area less than 90 $Å^2$ is usually needed and molecules with a polar surface area of greater than 120–140 $Å^2$ tend to be poor in permeating cell membranes.[35]

Conclusion

In summary, to develop new drugs for the treatment of Alzheimer's disease, a small library of 28 new triazolothiadiazole and triazolothiadiazine compounds was designed and synthesized. The structural build-up was established on the basis of spectro-analytical methods and, in case of **4i** and **5e**, by X-ray crystallography. The newly synthesized triazolothiadiazoles (**4a–l**) and triazolothiadiazines (**5a–p**) were evaluated for their cholinesterase inhibition against EeAChE and hBChE by Ellman's method using neostigmine and donepezil as standard inhibitors. Among the screened derivatives, **4j** emerged as a lead candidate showing highest inhibition with IC_{50} value of 0.117 ± 0.007 μM, which is ~139-fold strong inhibition as compared to neostigmine. This compound incorporated a bromo substituent at the meta-position of the phenyl ring attached at C-3 along with 4-methyl substituent at the *para*-position of the aromatic ring attached at C-6 of triazolothiadiazole core. In the triazolothiadiazine series, **5j** and **5e** depicted a clear selectivity towards EeAChE with IC_{50} values of 0.065 ± 0.005 and 0.075 ± 0.001 μM, respectively, which is ~250- and ~218-fold stronger inhibition as compared to neostigmine (IC_{50} = 16.3 ± 1.12 μM), whereas, compound **5d** was the lead candidate against BChE with IC_{50} value of 0.066 ± 0.021 μM (~427- and 109-fold stronger inhibition) as compared to neostigmine and donepezil, respectively. Overall, these heteroaromatic structures with substituted aryl rings installed at 3- and 6-position have emerged as highly promising anti-Alzheimer drug candidates with potent inhibitory efficacy.

In addition, the synthesized compounds were also tested for their monoamine oxidase (MAO) inhibition. Among triazolothiadiazole series, **4a** delivered highest potency against MAO-A with IC_{50} value of 0.11 ± 0.005 μM which is ~33-fold higher inhibition as compared to standard inhibitor, clorgyline (IC_{50} = 3.64 ± 0.012 μM), whereas, among triazolothiadiazine series, compound **5c** turned to be a lead candidate with IC_{50} value of 0.011 ± 0.001 μM which is ~330-fold strong inhibition as compared to the standard inhibitor, clorgyline. In general, the synthesized compounds were more potent and selective towards MAO-A, opening the possibility of rational design of more potent and selective inhibitors of monoamine oxidases (MAO). Computational analysis revealed plausible putative binding modes of the extended structure of **4k** and **5d** along the active site gorge of AChE and BuChE. These inhibitors can be considered as promising lead for further investigations for the treatment of AD.

Experimental

General

Unless otherwise noted, all materials were obtained from commercial suppliers (Aldrich and Alfa aesar companies) and used without further purification. Thin layer chromatography (TLC) was performed on Merck DF-Alufoilien $60F_{254}$ 0.2 mm precoated plates. Product spots were visualized under UV light at 254 and 365 nm. Melting points were recorded on a Stuart melting point apparatus (SMP3) and are uncorrected. Infra-red (IR) spectra were recorded on FTS 3000 MX, Bio-Rad Merlin (Excalibur model) spectrophotometer. ^{1}H NMR spectra were recorded on a Bruker Avance (300 MHz) spectrometer. Chemical shifts (δ) are quoted in parts per million (ppm) downfield of tetramethylsilane, using residual solvent as internal standard (DMSO-d_6 at 2.50 ppm). Proton-decoupled ^{13}CNMR spectra were recorded on a Bruker Avance (75 MHz) spectrometer using deuterated solvent as internal standard (DMSO-d_6 at 39.52 ppm). The elemental analysis was performed on Leco CHNS-932 Elemental Analyzer, Leco Corporation (USA). Abbreviations used in the description of resonances are: s (singlet), d (doublet), t (triplet), q (quartet), m (multiplet), Ar (aromatic).

Preparation of 4-amino-1,2,4-triazole-3-thiol (3a,b)

A mixture of corresponding benzoic acid (1.0 mmol) and thiocarbohydrazide (1.5 mmol) was heated in a sand bath at 190–200 °C for 1 h. The product obtained on cooling was triturated with hot water, filtered, dried, and recrystallized (ethanol) to afford corresponding 4-amino-1,2,4-triazole-3-thiol.[30]

4-Amino-5-(4-methoxyphenyl)-4*H*-1,2,4-triazole-3-thiol (3a). White solid (80%, 177 mg): mp 210–211 °C; R_f: 0.62 (10% MeOH/$CHCl_3$); IR (ATR, cm^{-1}): 3015 (Ar-H), 2937, 2824 (CH_3), 2554 (SH), 1602 (C=N), 1546, 1511 (C=C); ^1H NMR (300 MHz, DMSO-d_6): δ 13.83 (s, 1H, SH), 7.99 (d, 2H, J = 8.7 Hz, Ar-H), 7.07 (d, 2H, J = 8.7 Hz, Ar-H), 5.77 (s, 2H, NH_2), 3.81 (s, 3H, OCH_3); ^{13}C NMR (75 MHz, DMSO-d_6): δ 167.03, 161.28, 149.76, 130.05, 118.53, 114.40, 55.81. Analysis calcd for $C_9H_{10}N_4OS$ (222.06): C, 48.63; H, 4.53; N, 25.21; S, 14.43. Found: C, 48.54; H, 4.43; N, 25.18; S, 14.30.

4-Amino-5-(3-bromophenyl)-4*H*-1,2,4-triazole-3-thiol (3b). White solid (81%, 219 mg): mp 226–227 °C; R_f: 0.65 (10% MeOH/$CHCl_3$); IR (ATR, cm^{-1}): 3035 (Ar-H), 2942, 2857 (CH_2), 2563 (SH), 1605 (C=N), 1567, 1521 (C=C); ^1H NMR (300 MHz, DMSO-d_6): δ 14.03 (s, 1H, SH), 8.28–8.27 (m, 1H, Ar-H), 8.01 (d, 1H, J = 8.1 Hz, Ar-H), 7.76–7.73 (m, 1H, Ar-H), 7.49 (t, 1H, J = 7.8 Hz, Ar-H), 5.80 (s, 2H, NH_2); ^{13}C NMR (75 MHz, DMSO-d_6): δ 167.72, 148.49, 133.66, 131.22, 130.84, 128.33, 127.39, 122.08. Analysis calcd for $C_8H_7BrN_4S$ (269.96): C, 35.44; H, 2.60; N, 20.66; S, 11.83. Found: C, 35.29; H, 2.49; N, 20.57; S, 11.76.

Preparation of 1,2,4-triazolo[3,4-*b*][1,3,4]thiadiazoles (4a–l)

A mixture of corresponding 4-amino-1,2,4-triazole-3-thiol (**3a,b**) (1.0 mmol) and substituted aryloxy acids (1.1 mmol) in $POCl_3$ (5 mL) was refluxed for 6 h. The reaction mixture was slowly poured into crushed ice with stirring and neutralized with sodium bicarbonate. Solid material was filtered, washed with cold water, dried, and recrystallized (ethanol) to afford 1,2,4-triazolo[3,4-*b*][1,3,4]thiadiazoles (**4a–l**).[28,29]

2-((3-(4-Methoxyphenyl)-[1,2,4]triazolo[3,4-*b*][1,3,4]thiadiazol-6-yl)methoxy)phenol (4a). Purple solid (78%, 276 mg): mp 238–239 °C; R_f: 0.72 (10% MeOH/$CHCl_3$); IR (ATR, cm^{-1}): 3425 (OH), 3009 (Ar-H), 2938, 2803 (CH_3), 1610 (C=N), 1565, 1502 (C=C); ^1H NMR (300 MHz, DMSO-d_6): δ 8.13 (d, 2H, J = 8.7 Hz, Ar-H), 7.96 (d, 2H, J = 9.0 Hz, Ar-H), 7.17–7.04 (m, 3H, Ar-H), 6.93 (t, 1H, J = 5.7 Hz, Ar-H), 5.78 (s, 2H, OCH_2), 5.56 (s, 1H, OH), 3.83 (s, 3H, OCH_3); ^{13}C NMR (75 MHz, DMSO-d_6): δ 169.23, 166.87, 161.25, 152.55, 149.70, 145.84, 130.05, 129.91, 127.93, 125.71, 118.51, 118.28, 114.40, 65.85, 55.84. Analysis calcd for $C_{17}H_{14}N_4O_3S$ (354.08): C, 57.62; H, 3.98; N, 15.81; S, 9.05. Found: C, 57.53; H, 3.74; N, 15.67; S, 8.90.

4-((3-(4-Methoxyphenyl)-[1,2,4]triazolo[3,4-*b*][1,3,4]thiadiazol-6-yl)methoxy)phenol (4b). Off-white solid (76%, 269 mg): mp 165–166 °C; R_f: 0.71 (10% MeOH/$CHCl_3$); IR (ATR, cm^{-1}): 3412 (OH), 3029 (Ar-H), 2946, 2839 (CH_3), 1608 (C=N), 1547, 1502 (C=C);^1H NMR (300 MHz, DMSO-d_6): δ 8.11 (d, 2H, J = 9.0 Hz, Ar-H), 7.15–7.01 (m, 6H, Ar-H), 5.55 (s, 2H, OCH_2), 5.52 (s, 1H, OH), 3.82 (s, 3H, OCH_3); ^{13}C NMR (75 MHz, DMSO-d_6): δ 168.50, 168.40, 161.23, 153.33, 147.49, 145.67, 127.93, 121.66, 121.26, 116.24, 115.05, 65.86, 55.87. Analysis calcd for $C_{17}H_{14}N_4O_3S$ (354.08): C, 57.62; H, 3.98; N, 15.81; S, 9.05. Found: C, 57.54; H, 3.79; N, 15.70; S, 9.17.

3-(4-Methoxyphenyl)-6-(*o*-tolyloxymethyl)-[1,2,4]triazolo[3,4-*b*][1,3,4]thiadiazole (4c). Brown solid (72%, 253 mg): mp 151–152 °C; R_f: 0.68 (10% MeOH/$CHCl_3$); IR (ATR, cm^{-1}): 3019 (Ar-H), 2934, 2838 (CH_3), 1612 (C=N), 1578, 1546 (C=C); ^1H NMR (300 MHz, DMSO-d_6): δ 8.14 (d, 2H, J = 8.7 Hz, Ar-H), 7.23–7.11 (m, 5H, Ar-H), 6.94 (t, 1H, J = 7.2 Hz, Ar-H), 5.60 (s, 2H, OCH_2), 3.84 (s, 3H, OCH_3), 2.62 (s, 3H, CH_3); ^{13}C NMR (75 MHz, DMSO-d_6): δ 168.78, 161.25, 155.60, 154.11, 145.66, 131.28, 127.91, 127.62, 126.57, 122.28, 118.28, 115.05, 112.65, 65.38, 55.85, 16.37. Analysis calcd for $C_{18}H_{16}N_4O_2S$ (352.10): C, 61.35; H, 4.58; N, 15.90; S, 9.10. Found: C, 61.17; H, 4.42; N, 15.73; S, 9.03.

3-(4-Methoxyphenyl)-6-(*p*-tolyloxymethyl)-[1,2,4]triazolo[3,4-*b*][1,3,4]thiadiazole (4d). Brown solid (74%, 260 mg): mp 148–149 °C; R_f: 0.67 (10% MeOH/$CHCl_3$); IR (ATR, cm^{-1}): 3015 (Ar-H), 2923, 2838 (CH_3), 1610 (C=N), 1547, 1508 (C=C); ^1H NMR (300 MHz, DMSO-d_6): δ 8.12 (d, 2H, J = 8.7 Hz, Ar-H), 7.16–7.12 (m, 4H, Ar-H), 7.01 (d, 2H, J = 8.7 Hz, Ar-H), 5.55 (s, 2H, OCH_2), 3.83 (s, 3H, OCH_3), 2.23 (s, 3H, CH_3); ^{13}C NMR (75 MHz, DMSO-d_6): δ 168.49, 161.23, 155.40, 154.16, 145.64, 131.44, 130.52, 127.90, 118.26, 115.39, 115.02, 65.40, 55.83, 20.54. Analysis calcd for $C_{18}H_{16}N_4O_2S$ (352.10): C, 61.35; H, 4.58; N, 15.90; S, 9.10. Found: C, 61.53; H, 4.39; N, 15.74; S, 9.24.

6-((4-Methoxyphenoxy)methyl)-3-(4-methoxyphenyl)-[1,2,4]-triazolo[3,4-*b*][1,3,4]thiadiazole (4e). Light brown solid (81%, 298 mg): mp 133–134 °C; R_f: 0.64 (10% MeOH/$CHCl_3$); IR (ATR, cm^{-1}): 3045 (Ar-H), 2935, 2834 (CH_3), 1611 (C=N), 1548, 1505 (C=C); ^1H NMR (300 MHz, DMSO-d_6): δ 8.13 (d, 2H, J = 8.7 Hz, Ar-H), 7.15 (d, 2H, J = 8.7 Hz, Ar-H), 7.07 (d, 2H, J = 9.0 Hz, Ar-H), 6.90 (d, 2H, J = 9.0 Hz, Ar-H), 5.53 (s, 2H, OCH_2), 3.83 (s, 3H, OCH_3), 3.70 (s, 3H, OCH_3); ^{13}C NMR (75 MHz, DMSO-d_6): δ 168.62, 161.24, 154.90, 154.18, 151.43, 145.65, 127.91, 118.25, 116.75, 115.21, 115.04, 66.01, 55.85, 55.83. Analysis calcd for $C_{18}H_{16}N_4O_3S$ (368.09): C, 58.68; H, 4.38; N, 15.21; S, 8.70. Found: C, 58.53; H, 4.29; N, 15.32; S, 8.56.

6-((4-Fluorophenoxy)methyl)-3-(4-methoxyphenyl)-[1,2,4]triazolo[3,4-*b*][1,3,4]thiadiazole (4f). Brown solid (76%, 270 mg): mp 137–138 °C; R_f: 0.67 (10% MeOH/$CHCl_3$); IR (ATR, cm^{-1}): 3050 (Ar-H), 2931, 2837 (CH_3), 1612 (C=N), 1552, 1504 (C=C); ^1H NMR (300 MHz, DMSO-d_6): δ 8.11 (d, 2H, J = 8.7 Hz, Ar-H), 7.46 (bs, 2H, Ar-H), 7.18–7.12 (m, 4H, Ar-H), 5.58 (s, 2H, OCH_2), 3.82 (s, 3H, OCH_3); ^{13}C NMR (75 MHz, DMSO-d_6): δ 168.03, 161.23, 159.37, 156.22, 154.20, 153.82, 145.66, 127.90, 118.22, 117.19, 117.08, 116.76, 116.45, 115.03, 65.97, 55.85. Analysis calcd for $C_{17}H_{13}FN_4O_2S$ (356.07): C, 57.29; H, 3.68; N, 15.72; S, 9.00. Found: C, 57.43; H, 3.46; N, 15.56; S, 9.09.

2-((3-(3-Bromophenyl)-[1,2,4]triazolo[3,4-*b*][1,3,4]thiadiazol-6-yl)methoxy)phenol (4g). Brown solid (76%, 305 mg): mp 246–247 °C; R_f: 0.78 (10% MeOH/$CHCl_3$); IR (ATR, cm^{-1}): 3416 (OH), 3037 (Ar-H), 2945, 2855 (CH_3), 1603 (C=N), 1556, 1510 (C=C); ^1H NMR (300 MHz, DMSO-d_6): δ 14.03 (s, 1H, OH), 8.28 (s, 1H, Ar-H), 8.01 (d, 1H, J = 7.8 Hz, Ar-H), 7.76 (d, 1H, J = 7.8 Hz, Ar-H), 7.53–7.47 (t, 2H, J = 7.8 Hz, Ar-H), 7.25–7.16 (m, 1H, Ar-H), 7.12–6.94 (m, 2H, Ar-H), 5.80 (s, 2H, OCH_2); ^{13}C NMR (75 MHz, DMSO-d_6): δ 168.44, 161.70, 156.23, 151.54, 146.38,

142.87, 135.50, 132.65, 129.87, 128.54, 126.32, 125.12, 116.77, 112.68, 111.09, 65.38. Analysis calcd for $C_{16}H_{11}BrN_4O_2S$ (401.98): C, 47.66; H, 2.75; N, 13.89; S, 7.95. Found: C, 47.50; H, 2.53; N, 13.71; S, 7.78.

4-((3-(3-Bromophenyl)-[1,2,4]triazolo[3,4-*b*][1,3,4]thiadiazol-6-yl)methoxy)phenol (4h). Brown solid (75%, 301 mg): mp 148–149 °C; R_f: 0.76 (10% MeOH/$CHCl_3$); IR (ATR, cm^{-1}): 3412 (OH), 3030 (Ar-H), 2932, 2838 (CH_3), 1609 (C=N), 1567, 1515 (C=C); ^1H NMR (300 MHz, DMSO-d_6): δ 14.06 (s, 1H, OH), 8.33 (bs, 1H, Ar-H), 8.20 (d, 1H, J = 8.1 Hz, Ar-H), 7.76 (d, 1H, J = 8.1 Hz, Ar-H), 7.59–7.54 (m, 1H, Ar-H), 7.25–7.16 (m, 2H, Ar-H), 7.12–6.94 (m, 2H, Ar-H), 5.65 (s, 2H, OCH_2); ^{13}C NMR (75 MHz, DMSO-d_6): δ 168.34, 161.87, 156.65, 151.76, 146.34, 142.87, 135.58, 132.98, 129.09, 128.06, 125.32, 125.19, 118.67, 65.38. Analysis calcd for $C_{16}H_{11}BrN_4O_2S$ (401.98): C, 47.66; H, 2.75; N, 13.89; S, 7.95. Found: C, 47.53; H, 2.57; N, 13.72; S, 7.80.

3-(3-Bromophenyl)-6-(*o*-tolyloxymethyl)-[1,2,4]triazolo[3,4-*b*]-[1,3,4]thiadiazole (4i). Off-white solid (74%, 296 mg): mp 218–219 °C; R_f: 0.73 (10% MeOH/$CHCl_3$); IR (ATR, cm^{-1}): 3050 (Ar-H), 2957, 2830 (CH_3), 1603 (C=N), 1565, 1534 (C=C); ^1H NMR (300 MHz, DMSO-d_6): δ 8.37 (bs, 1H, Ar-H), 8.22 (d, 1H, J = 8.1 Hz, Ar-H), 7.78 (d, 1H, J = 8.4 Hz, Ar-H), 7.59 (t, 1H, J = 8.1 Hz, Ar-H), 7.24–7.13 (m, 3H, Ar-H), 6.95 (t, 1H, J = 6.6 Hz, Ar-H), 5.66 (s, 2H, OCH_2), 2.27 (s, 3H, CH_3); ^{13}C NMR (75 MHz, DMSO-d_6): δ 168.26, 161.77, 156.24, 150.54, 145.34, 142.87, 133.53, 132.57, 129.98, 128.45, 126.55, 125.72, 117.53, 112.68, 111.09, 65.38, 16.40. Analysis calcd for $C_{17}H_{13}BrN_4OS$ (400.00): C, 50.88; H, 3.27; N, 13.96; S, 7.99. Found: C, 50.69; H, 3.11; N, 13.77; S, 7.84.

3-(3-Bromophenyl)-6-(*p*-tolyloxymethyl)-[1,2,4]triazolo[3,4-*b*]-[1,3,4]thiadiazole (4j). Green solid (70%, 280 mg): mp 138–139 °C; R_f: 0.74 (10% MeOH/$CHCl_3$); IR (ATR, cm^{-1}): 3064 (Ar-H), 2912, 2837 (CH_3), 1606 (C=N), 1556, 1522 (C=C); ^1H NMR (300 MHz, DMSO-d_6): δ 8.34 (bs, 1H, Ar-H), 8.22 (d, 1H, J = 8.1 Hz, Ar-H), 7.77 (d, 1H, J = 8.1 Hz, Ar-H), 7.56 (t, 1H, J = 7.8 Hz, Ar-H), 7.45–7.42 (m, 2H, Ar-H), 7.24–7.19 (m, 2H, Ar-H), 5.60 (s, 2H, OCH_2), 2.24 (s, 3H, CH_3); ^{13}C NMR (75 MHz, DMSO-d_6): δ 168.87, 161.47, 155.29, 151.50, 145.87, 138.57, 133.80, 132.52, 128.18, 126.59, 124.62, 117.53, 112.60, 65.76, 16.49. Analysis calcd for $C_{17}H_{13}BrN_4OS$ (400.00): C, 50.88; H, 3.27; N, 13.96; S, 7.99. Found: C, 50.64; H, 3.36; N, 13.85; S, 7.79.

3-(3-Bromophenyl)-6-((4-methoxyphenoxy)methyl)-[1,2,4]triazolo[3,4-*b*][1,3,4]thiadiazole (4k). Brown solid (76%, 316 mg): mp 169–170 °C; R_f: 0.76 (10% MeOH/$CHCl_3$); IR (ATR, cm^{-1}): 3028 (Ar-H), 2945, 2835 (CH_3), 1599 (C=N), 1543, 1527 (C=C); ^1H NMR (300 MHz, DMSO-d_6): δ 8.35–8.32 (m, 1H, Ar-H), 8.22 (d, 1H, J = 8.1 Hz, Ar-H), 7.77 (d, 1H, J = 8.1 Hz, Ar-H), 7.57 (t, 1H, J = 7.8 Hz, Ar-H), 7.16–6.77 (m, 4H, Ar-H), 5.57 (s, 2H, OCH_2), 3.70 (s, 3H, OCH_3); ^{13}C NMR (75 MHz, DMSO-d_6): δ 168.60, 161.57, 156.45, 150.34, 145.87, 142.87, 133.12, 129.76, 126.38, 125.62, 118.51, 115.68, 111.08, 65.34, 55.42. Analysis calcd for $C_{17}H_{13}BrN_4O_2S$ (415.99): C, 48.93; H, 3.14; N, 13.43; S, 7.68. Found: C, 48.73; H, 3.27; N, 13.31; S, 7.50.

3-(3-Bromophenyl)-6-((4-fluorophenoxy)methyl)-[1,2,4]triazolo-[3,4-*b*][1,3,4]thiadiazole (4l). Light brown solid (74%, 299 mg): mp 180–181 °C; R_f: 0.75 (10% MeOH/$CHCl_3$); IR (ATR, cm^{-1}): 3043 (Ar-H), 2948, 2832 (CH_2), 1604 (C=N), 1558, 1517 (C=C); ^1H NMR (300 MHz, DMSO-d_6): δ 8.34–8.31 (m, 1H, Ar-H), 8.20 (d, 1H, J = 7.8 Hz, Ar-H), 7.78.7.75 (m, 1H, Ar-H), 7.57 (t, 1H, J = 8.1 Hz, Ar-H), 7.20–7.16 (m, 4H, Ar-H), 5.63 (s, 2H, OCH_2); ^{13}C NMR (75 MHz, DMSO-d_6): δ 168.93, 159.39, 156.24, 155.26, 153.83, 153.80, 144.34, 133.51, 131.90, 128.43, 127.94, 125.17, 122.73, 117.18, 117.07, 116.78, 116.47, 65.92. Analysis calcd for $C_{16}H_{10}BrFN_4OS$ (403.97): C, 47.42; H, 2.49; N, 13.83; S, 7.91. Found: C, 47.53; H, 2.35; N, 13.74; S, 7.78.

Preparation of 1,2,4-triazolo[3,4-*b*][1,3,4]-thiadiazines (5a–p)

A mixture of corresponding 4-amino-1,2,4-triazole-3-thiol (**3a,b**) (1.0 mmol) and substituted phenacyl bromides (1.2 mmol) was refluxed in absolute ethanol (10 mL) for 7 h. The reaction mass was poured into crushed ice and neutralized with sodium bicarbonate. Solid product obtained was filtered, washed with water, dried, and recrystallized (ethanol) to afford conjugated products (**6a–p**).[28,29]

3,6-Bis(4-methoxyphenyl)-7*H*-[1,2,4]triazolo[3,4-*b*][1,3,4]-thiadiazine (5a). Off-white solid (81%, 285 mg): mp 174–175 °C; R_f: 0.72 (10% MeOH/$CHCl_3$); IR (ATR, cm^{-1}): 3066 (Ar-H), 2929, 2832 (CH_2), 1605 (C=N), 1541, 1513 (C=C); ^1H NMR (300 MHz, DMSO-d_6): δ 8.00–7.96 (m, 4H, Ar-H), 7.15–7.11 (m, 4H, Ar-H), 4.40 (s, 2H, SCH_2), 3.85 (s, 3H, OCH_3), 3.84 (s, 3H, OCH_3); ^{13}C NMR (75 MHz, DMSO-d_6): δ 162.75, 161.22, 155.99, 151.65, 142.62, 129.93, 129.91, 125.96, 115.04, 114.71, 56.03, 22.93. Analysis calcd for $C_{18}H_{16}N_4O_2S$ (352.10): C, 61.35; H, 4.58; N, 15.90; S, 9.10. Found: C, 61.26; H, 4.62; N, 15.78; S, 9.01.

6-(4-Chlorophenyl)-3-(4-methoxyphenyl)-7*H*-[1,2,4]triazolo-[3,4-*b*][1,3,4]thiadiazine (5b). White solid (83%, 295 mg): mp 210–211 °C; R_f: 0.68 (10% MeOH/$CHCl_3$); IR (ATR, cm^{-1}): 3034 (Ar-H), 2912, 2838 (CH_2), 1613 (C=N), 1548, 1487 (C=C); ^1H NMR (300 MHz, DMSO-d_6): δ 8.03–8.00 (m, 2H, Ar-H), 7.97–7.92 (m, 2H, Ar-H), 7.67–7.62 (m, 2H, Ar-H), 7.15–7.10 (m, 2H, Ar-H), 4.42 (s, 2H, SCH_2), 3.83 (s, 3H, OCH_3); ^{13}C NMR (75 MHz, DMSO-d_6): δ 161.21, 155.25, 151.96, 142.41, 137.23, 132.82, 129.96, 129.78, 129.67, 118.70, 114.71, 55.81, 23.07. Analysis calcd for $C_{17}H_{13}ClN_4OS$ (356.05): C, 57.22; H, 3.67; N, 15.70; S, 8.99. Found: C, 57.11; H, 3.54; N, 15.53; S, 9.08.

6-(4-Fluorophenyl)-3-(4-methoxyphenyl)-7*H*-[1,2,4]triazolo-[3,4-*b*][1,3,4]thiadiazine (5c). White solid (77%, 262 mg): mp 241–242 °C; R_f: 0.65 (10% MeOH/$CHCl_3$); IR (ATR, cm^{-1}): 3050 (Ar-H), 2952, 2848 (CH_2), 1603 (C=N), 1532, 1515 (C=C); ^1H NMR (300 MHz, DMSO-d_6): δ 8.08 (bs, 2H, Ar-H), 7.98 (d, 2H, J = 6.9 Hz, Ar-H), 7.42 (bs, 2H, Ar-H), 7.13 (d, 2H, J = 6.6 Hz, Ar-H), 4.42 (s, 2H, SCH_2), 3.84 (s, 3H, OCH_3); ^{13}C NMR (75 MHz, DMSO-d_6): δ 161.74, 161.17, 155.97, 151.69, 141.60, 133.76, 129.93, 125.96, 118.67, 115.34, 114.71, 55.83, 22.97. Analysis calcd for $C_{17}H_{13}FN_4OS$ (340.08): C, 59.99; H, 3.85; N, 16.46; S, 9.42. Found: C, 59.81; H, 3.76; N, 16.55; S, 9.31.

3-(4-Methoxyphenyl)-6-*p*-tolyl-7*H*-[1,2,4]triazolo[3,4-*b*][1,3,4]-thiadiazine (5d). Off-white solid (72%, 242 mg): mp 231–232 °C; R_f: 0.67 (10% MeOH/$CHCl_3$); IR (ATR, cm^{-1}): 3043 (Ar-H), 2975, 2854 (CH_2), 1607 (C=N), 1589, 1512 (C=C); ^1H NMR (300 MHz, DMSO-d_6): δ 7.98 (m, 4H, Ar-H), 7.39 (d, 2H, J = 8.7 Hz, Ar-H), 7.17 (d, 2H, J = 9.0 Hz, Ar-H), 4.45 (s, 2H, SCH_2), 3.84 (s, 3H, OCH_3); ^{13}C NMR (75 MHz, DMSO-d_6): δ 161.64, 157.12, 151.46,

143.22, 142.96, 130.90, 130.28, 130.22, 128.08, 117.62, 114.85, 55.92, 23.12, 21.54. Analysis calcd for $C_{18}H_{16}N_4OS$ (336.10): C, 64.26; H, 4.79; N, 16.65; S, 9.53. Found: C, 64.09; H, 4.66; N, 16.81; S, 9.40.

3-(4-Methoxyphenyl)-6-(biphen-1-yl)-7*H*-[1,2,4]triazolo[3,4-*b*]-[1,3,4]thiadiazine (5e). Light yellow solid (80%, 318 mg): mp 208–209 °C; R_f: 0.68 (10% MeOH/$CHCl_3$); IR (ATR, cm^{-1}): 3037 (Ar-H), 2917, 2848 (CH_2), 1603 (C=N), 1573, 1509 (C=C); ^1H NMR (300 MHz, DMSO-d_6): δ 8.11 (d, 2H, J = 8.7 Hz, Ar-H), 8.00 (d, 2H, J = 8.7 Hz, Ar-H), 7.89 (d, 2H, J = 8.4 Hz, Ar-H), 7.77 (d, 2H, J = 8.4 Hz, Ar-H), 7.50 (d, 1H, J = 7.2 Hz, Ar-H), 7.46–7.39 (m, 2H, Ar-H), 7.17 (d, 2H, J = 8.7 Hz, Ar-H), 4.52 (s, 2H, SCH_2), 3.84 (s, 3H, OCH_3); ^{13}C NMR (75 MHz, DMSO-d_6): δ 161.68, 156.86, 151.53, 143.98, 139.15, 132.54, 130.36, 130.22, 129.60, 128.87, 128.79, 127.74, 127.35, 117.51, 114.87, 55.92, 23.18. Analysis calcd for $C_{23}H_{18}N_4OS$ (398.12): C, 69.32; H, 4.55; N, 14.06; S, 8.05. Found: C, 69.17; H, 4.67; N, 13.94; S, 8.01.

3-(4-Methoxyphenyl)-6-(naphthalen-1-yl)-7*H*-[1,2,4]triazolo-[3,4-*b*][1,3,4]thiadiazine (5f). White solid (75%, 279 mg): mp 221–222 °C; R_f: 0.66 (10% MeOH/$CHCl_3$); IR (ATR, cm^{-1}): 3056 (Ar-H), 2928, 2835 (CH_2), 1614 (C=N), 1581, 1537 (C=C); ^1H NMR (300 MHz, DMSO-d_6): δ 8.65 (bs, 1H, Ar-H), 8.13–8.06 (m, 3H, Ar-H), 8.02 (d, 3H, J = 9.0 Hz, Ar-H), 7.69–7.62 (m, 2H, Ar-H), 7.16 (d, 2H, J = 8.7 Hz, Ar-H), 4.58 (s, 2H, SCH_2), 3.85 (s, 3H, OCH_3); ^{13}C NMR (75 MHz, DMSO-d_6): δ 161.23, 156.08, 152.00, 142.53, 134.70, 132.91, 131.26, 129.96, 129.64, 129.46, 129.35, 128.79, 128.23, 127.67, 123.66, 118.86, 114.76, 55.83, 23.05. Analysis calcd for $C_{21}H_{16}N_4OS$ (372.10): C, 67.72; H, 4.33; N, 15.09; S, 8.61. Found: C, 67.64; H, 4.43; N, 14.96; S, 8.49.

3-(4-Methoxyphenyl)-6-(4-nitrophenyl)-7*H*-[1,2,4]triazolo[3,4-*b*][1,3,4]thiadiazine (5g). Yellow solid (79%, 290 mg): mp 274–275 °C; R_f: 0.67 (10% MeOH/$CHCl_3$); IR (ATR, cm^{-1}): 3013 (Ar-H), 2932, 2840 (CH_2), 1610 (C=N), 1580, 1518 (C=C); ^1H NMR (300 MHz, DMSO-d_6): δ 8.41 (d, 2H, J = 9.0 Hz, Ar-H), 8.25 (d, 2H, J = 9.0 Hz, Ar-H), 7.95 (d, 2H, J = 8.7 Hz, Ar-H), 7.15 (d, 2H, J = 9.0 Hz, Ar-H), 4.50 (s, 2H, SCH_2), 3.84 (s, 3H, OCH_3); ^{13}C NMR (75 MHz, DMSO-d_6): δ 161.43, 156.18, 152.55, 142.59, 140.27, 138.25, 134.78, 132.85, 129.65, 129.16, 128.65, 55.84, 23.35. Analysis calcd for $C_{17}H_{13}N_5O_3S$ (367.07): C, 55.58; H, 3.57; N, 19.06; S, 8.73. Found: C, 55.53; H, 3.66; N, 18.85; S, 8.61.

6-(3,4-Dichlorophenyl)-3-(4-methoxyphenyl)-7*H*-[1,2,4]triazolo-[3,4-*b*][1,3,4]thiadiazine (5h). Light yellow solid (74%, 288 mg): mp 268–269 °C; R_f: 0.69 (10% MeOH/$CHCl_3$); IR (ATR, cm^{-1}): 3010 (Ar-H), 2920, 2838 (CH_2), 1608 (C=N), 1547, 1536 (C=C); ^1H NMR (300 MHz, DMSO-d_6): δ 8.07–8.00 (m, 2H, Ar-H), 7.95 (d, 2H, J = 8.7 Hz, Ar-H), 7.90 (s, 1H, Ar-H), 7.15 (d, 2H, J = 9.0 Hz, Ar-H), 4.52 (s, 2H, SCH_2), 3.84 (s, 3H, OCH_3); ^{13}C NMR (75 MHz, DMSO-d_6): δ 161.46, 156.18, 152.55, 149.66, 145.84, 145.41, 142.76, 140.56, 138.47, 134.73, 132.87, 129.57, 124.65, 55.83, 23.21. Analysis calcd for $C_{17}H_{12}Cl_2N_4OS$ (390.01): C, 52.18; H, 3.09; N, 14.32; S, 8.20. Found: C, 52.34; H, 3.02; N, 14.38; S, 8.04.

3-(3-Bromophenyl)-6-(4-methoxyphenyl)-7*H*-[1,2,4]triazolo-[3,4-*b*][1,3,4]thiadiazine (5i). White solid (81%, 324 mg): mp 231–232 °C; R_f: 0.70 (10% MeOH/$CHCl_3$); IR (ATR, cm^{-1}): 3028 (Ar-H), 2934, 2834 (CH_2), 1608 (C=N), 1586, 1514 (C=C); ^1H NMR (300 MHz, DMSO-d_6): δ 8.21 (d, 1H, J = 1.5 Hz, Ar-H), 8.04 (d, 1H, J = 7.8 Hz, Ar-H), 7.99 (d, 2H, J = 9.0 Hz, Ar-H), 7.75 (d, 1H, J = 8.7 Hz, Ar-H), 7.54 (t, 1H, J = 8.1 Hz, Ar-H), 7.13 (d, 2H, J = 8.7 Hz, Ar-H), 4.41 (s, 2H, SCH_2), 3.85 (s, 3H, OCH_3); ^{13}C NMR (75 MHz, DMSO-d_6): δ 162.86, 156.28, 150.43, 143.53, 133.26, 131.46, 130.69, 129.91, 128.63, 127.11, 125.80, 122.25, 115.06, 56.06, 23.00. Analysis calcd for $C_{17}H_{13}BrN_4S$ (400.00): C, 50.88; H, 3.27; N, 13.96; S, 7.99. Found: C, 50.69; H, 3.12; N, 13.80; S, 7.78.

3-(3-Bromophenyl)-6-(4-chlorophenyl)-7*H*-[1,2,4]triazolo[3,4-*b*][1,3,4]thiadiazine (5j). White solid (80%, 323 mg): mp 281–282 °C; R_f: 0.72 (10% MeOH/$CHCl_3$); IR (ATR, cm^{-1}): 3037 (Ar-H), 2933, 2837 (CH_2), 1596 (C=N), 1587, 1556 (C=C); ^1H NMR (300 MHz, DMSO-d_6): δ 8.21–8.20 (m, 1H, Ar-H), 8.13–8.10 (m, 2H, Ar-H), 8.04 (d, 1H, J = 7.8 Hz, Ar-H), 7.75 (d, 1H, J = 8.7 Hz, Ar-H), 7.67–7.62 (m, 2H, Ar-H), 7.54 (t, 1H, J = 8.1 Hz, Ar-H), 4.46 (s, 2H, SCH_2); ^{13}C NMR (75 MHz, DMSO-d_6): δ 162.88, 155.28, 151.40, 142.59, 137.66, 137.28, 132.47, 130.59, 129.99, 126.64, 124.82, 122.76, 115.67, 23.08. Analysis calcd for $C_{16}H_{10}BrClN_4S$ (403.95): C, 47.37; H, 2.48; N, 13.81; S, 7.90. Found: C, 47.24; H, 2.27; N, 13.96; S, 7.74.

3-(3-Bromophenyl)-6-(4-fluorophenyl)-7*H*-[1,2,4]triazolo[3,4-*b*][1,3,4]thiadiazine (5k). White solid (78%, 302 mg): mp 256–257 °C; R_f: 0.71 (10% MeOH/$CHCl_3$); IR (ATR, cm^{-1}): 3050 (Ar-H), 2938, 2847 (CH_2), 1601 (C=N), 1567, 1513 (C=C); ^1H NMR (300 MHz, DMSO-d_6): δ 8.21–8.20 (m, 1H, Ar-H), 8.08 (m, 2H, Ar-H), 8.04 (d, 1H, J = 7.8 Hz, Ar-H), 7.75 (d, 1H, J = 8.7 Hz, Ar-H), 7.42 (m, 2H, Ar-H), 7.54 (t, 1H, J = 8.1 Hz, Ar-H), 4.45 (s, 2H, SCH_2); ^{13}C NMR (75 MHz, DMSO-d_6): δ 162.67, 155.88, 151.49, 142.87, 137.65, 137.28, 132.47, 130.45, 129.95, 126.84, 125.11, 124.82, 124.78, 122.76, 121.54, 115.65, 23.44. Analysis calcd for $C_{16}H_{10}BrFN_4S$ (387.98): C, 49.37; H, 2.59; N, 14.39; S, 8.24. Found: C, 49.24; H, 2.67; N, 14.26; S, 8.12.

3-(3-Bromophenyl)-6-*p*-tolyl-7*H*-[1,2,4]triazolo[3,4-*b*][1,3,4]-thiadiazine (5l). White solid (73%, 280 mg): mp 245–246 °C; R_f: 0.69 (10% MeOH/$CHCl_3$); IR (ATR, cm^{-1}): 3033 (Ar-H), 2914, 2838 (CH_2), 1591 (C=N), 1562, 1521 (C=C); ^1H NMR (300 MHz, DMSO-d_6): δ 8.19–8.17 (m, 1H, Ar-H), 8.02 (d, 1H, J = 7.8 Hz, Ar-H), 7.92 (d, 2H, J = 8.7 Hz, Ar-H), 7.74 (d, 1H, J = 8.4 Hz, Ar-H), 7.53 (t, 1H, J = 7.8 Hz, Ar-H), 7.39 (d, 2H, J = 8.7 Hz, Ar-H), 4.48 (s, 2H, SCH_2), 2.38 (s, 3H, CH_3); ^{13}C NMR (75 MHz, DMSO-d_6): δ 161.76, 155.65, 151.96, 142.34, 136.39, 134.18, 130.08, 129.17, 125.10, 124.72, 122.46, 121.54, 115.63, 23.07, 21.32. Analysis. calcd for $C_{17}H_{13}BrN_4S$ (384.00): C, 53.00; H, 3.40; N, 14.54; S, 8.32. Found: C, 52.88; H, 3.62; N, 14.43; S, 8.17.

3-(3-Bromophenyl)-6-(biphenyl-1-yl)-7*H*-[1,2,4]triazolo[3,4-*b*]-[1,3,4]thiadiazine (5m). Off-white solid (77%, 343 mg): mp 206–207 °C; R_f: 0.67 (10% MeOH/$CHCl_3$); IR (ATR, cm^{-1}): 3025 (Ar-H), 2925, 2834 (CH_2), 1604 (C=N), 1589, 1549 (C=C); ^1H NMR (300 MHz, DMSO-d_6): δ 8.23–8.21 (m, 1H, Ar-H), 8.11–8.04 (m, 3H, Ar-H), 7.88 (d, 2H, J = 8.4 Hz, Ar-H), 7.78–7.75 (m, 3H, Ar-H), 7.56 (d, 2H, J = 7.8 Hz, Ar-H), 7.50 (t, 1H, J = 7.5 Hz, Ar-H), 7.42 (t, 1H, J = 6.9 Hz, Ar-H), 4.48 (s, 2H, SCH_2); ^{13}C NMR (75 MHz, DMSO-d_6): δ 156.34, 150.64, 143.93, 143.56, 139.14, 133.37, 132.63, 131.49, 130.77, 129.56, 128.84, 128.67, 128.53, 127.70, 127.36, 127.21, 122.30, 23.17. Analysis calcd for

$C_{22}H_{15}BrN_4S$ (446.02): C, 59.07; H, 3.38; N, 12.52; S, 7.17. Found: C, 58.93; H, 3.54; N, 12.34; S, 7.03.

3-(3-Bromophenyl)-6-(naphthalen-1-yl)-7*H*-[1,2,4]triazolo-[3,4-*b*][1,3,4]thiadiazine (5n). White solid (72%, 302 mg): mp 254–255 °C; R_f: 0.65 (10% MeOH/$CHCl_3$); IR (ATR, cm^{-1}): 3000 (Ar-H), 2920, 2844 (CH_2), 1630 (C=N), 1567, 1519 (C=C); ^1H NMR (300 MHz, DMSO-d_6): δ 8.65 (bs, 1H, Ar-H), 8.23–8.21 (m, 2H, Ar-H), 8.13–8.06 (m, 3H, Ar-H), 8.02 (d, 1H, $J = 9.0$ Hz, Ar-H), 7.77 (d, 1H, $J = 8.4$ Hz, Ar-H), 7.69–7.62 (m, 2H, Ar-H), 7.54 (t, 1H, $J = 7.8$ Hz, Ar-H), 4.58 (s, 2H, SCH_2); ^{13}C NMR (75 MHz, DMSO-d_6): δ 161.23, 156.08, 152.09, 145.87, 142.53, 134.56, 132.91, 131.37, 129.96, 129.56, 129.46, 129.35, 128.84, 128.67, 128.23, 127.70, 123.66, 118.30, 114.76, 23.05. Analysis calcd for $C_{20}H_{13}BrN_4S$ (420.00): C, 57.02; H, 3.11; N, 13.30; S, 7.61. Found: C, 56.89; H, 3.26; N, 13.18; S, 7.47.

3-(3-Bromophenyl)-6-(4-nitrophenyl)-7*H*-[1,2,4]triazolo[3,4-*b*][1,3,4]thiadiazine (5o). Light yellow solid (82%, 340 mg): mp 275–276 °C; R_f: 0.68 (10% MeOH/$CHCl_3$); IR (ATR, cm^{-1}): 3026 (Ar-H), 2933, 2857 (CH_2), 1607 (C=N), 1525, 1494 (C=C); ^1H NMR (300 MHz, DMSO-d_6): δ 8.41 (d, 2H, $J = 7.5$ Hz, Ar-H), 8.24 (d, 2H, $J = 7.5$ Hz, Ar-H), 8.16 (bs, 1H, Ar-H), 8.01 (d, 1H, $J = 6.9$ Hz, Ar-H), 7.77 (d, 1H, $J = 6.9$ Hz, Ar-H), 7.56 (t, 1H, $J = 7.2$ Hz, Ar-H), 4.51 (s, 2H, SCH_2); ^{13}C NMR (75 MHz, DMSO-d_6): δ 161.87, 156.29, 150.47, 145.66, 142.50, 133.76, 131.48, 130.69, 128.99, 128.67, 127.16, 125.80, 122.25, 23.42. Analysis calcd for $C_{16}H_{10}BrN_5O_2S$ (414.97): C, 46.17; H, 2.42; N, 16.82; S, 7.70. Found: C, 45.98; H, 2.27; N, 16.97; S, 7.54.

3-(3-Bromophenyl)-6-(3,4-dichlorophenyl)-7*H*-[1,2,4]triazolo-[3,4-*b*][1,3,4]thiadiazine (5p). White solid (79%, 346 mg): mp 285–286 °C; R_f: 0.70 (10% MeOH/$CHCl_3$); IR (ATR, cm^{-1}): 3034 (Ar-H), 2957, 2834 (CH_2), 1608 (C=N), 1556, 1508 (C=C); ^1H NMR (300 MHz, DMSO-d_6): δ 8.24 (bs, 1H, Ar-H), 8.16 (d, 1H, $J =$ 8.1 Hz, Ar-H), 7.95 (d, 2H, $J = 6.9$ Hz, Ar-H), 7.90 (s, 1H, Ar-H), 7.78 (d, 1H, $J = 8.4$ Hz, Ar-H), 7.54 (t, 1H, $J = 7.2$ Hz, Ar-H), 4.51 (s, 2H, SCH_2); ^{13}C NMR (75 MHz, DMSO-d_6): δ 161.46, 156.28, 152.47, 149.65, 145.60, 140.59, 138.71, 135.74, 130.69, 129.43, 128.67, 126.32, 125.88, 122.25, 118.54, 23.12. Analysis calcd for $C_{16}H_9BrCl_2N_4S$ (437.91): C, 43.66; H, 2.06; N, 12.73; S, 7.29. Found: C, 43.53; H, 1.96; N, 12.85; S, 7.10.

Pharmacological protocols

Cholinesterase inhibition assay. For the determination of cholinesterase inhibition, electric eel and horse serum were used as source of AChE and BChE, respectively. AChE and BChE inhibition was measured *in vitro* by the Ellman's spectrophotometric method with slight modification.[33] Reaction started by mixing 20 μL assay buffer, 10 μL of test compound and 10 μL of enzymes (0.5 and 3.4 U/mg of AChE or BChE, respectively). Then reaction mixture was incubated for 10 min at 25 °C. At the end of the pre-incubation period, 10 μL of 1 mM acetylthiocholine iodide or butyrylthiocholine chloride were added to the respective AChE or BChE enzyme solution and 50 μL of 0.5 mM, 5,5′-dithiobis-2-nitrobenzoic Acid (DTNB) was added as coloring reagent. The mixtures were incubated for 15 min at 25 °C. The formation of enzymatic product was determined by the variation in absorbance measured at 405 nm with microplate reader (Bio-Tek ELx800 TM, Instruments Inc., Winooski, VT, USA). In this bioactivity assay, the standard drugs, neostigmine and donepezil were used. The buffer for enzyme dilution comprised of 50 mM Tris–HCl containing 0.1% (w/v) BSA (pH 8). To remove the effect the DMSO on enzymes an blank assay was performed without any enzyme and accounted as non-enzymatic reaction. The analysis of each concentration was done in triplicate and the IC_{50} values were calculated with the linear regression parameters. The computer program used for this purpose is GraphPad Prism 5.0 (San Diego, CA, USA).

Monoamine oxidase inhibition assay. Monoamine oxidase inhibitory activities of the synthesized compounds were evaluated using standard protocol.[34] Assays were performed in 200 μL final volume in 96 well plate. Rat liver mitochondria were pretreated for 15 min at room temperature with an aqueous solution of clorgyline (30 nM) or deprenyl (300 nM) to irreversibly block MAO-A or MAO-B activity, respectively. Test compounds (2 μL), dissolved in DMSO (100%), were added to 90 μL of mitochondrial preparation (25.0 μg of protein for rat MAO-A and 5.0 μg protein for rat MAO-B) and were incubated for 30 min prior to the addition of 90 μL of freshly prepared Amplex Red fluorogenic substrate. The Amplex Red reagent were used as follows, for a 96 well plate, 1.0 mg of Amplex Red, dissolved in 200 μL of DMSO (100%) and 100 μL of reconstituted horseradish peroxidase (HRP 200 U mL^{-1}) stock solution (kit vial + 1.0 mL of 50 mM sodium phosphate buffer) was added to 9700 μL of sodium phosphate buffer (250 mM, pH 7.4). The enzymatic reaction was started by the addition of 20 μL per well of an aqueous solution of the substrate *p*-tyramine (300 μM final concentration). Deprenyl and clorgyline (each in a final concentration of 1.0 μM) were used to determine non MAO-B and non MAO-A enzyme activity, respectively. Fluorescence measurements were performed over 45 min and the concentration response curves of clorgyline and deprenyl served as positive controls for the rat MAO-A and rat MAO-B assay, respectively.

Molecular modelling studies of cholinesterases

Structure selection and preparation. Molecular modeling studies were conducted to observe the interactions of the compounds against both AChE and BChE enzymes. In order to perform efficient modeling studies, high-resolution structures of both enzymes were selected from the Protein DataBank[36] and prepared for the modeling. A high-resolution crystal structure of 3.10 Å (PDB code: 4BDT) was selected for human acetylcholinesterase and a high-resolution crystal structure of 2.10 Å (PDB code: 4BDS) was selected for human butyrylcholinesterase. Both structures have well defined binding sites, as the X-ray structures for both enzymes are co-crystallized with bound inhibitors. The AChE was co-crystallized with huprine W (PDB ID: HUW) and BChE was co-crystallized with bound ligand tacrine (PDB ID: THA) that occupy the binding site of the enzyme.

Before studying the proteins in molecular modeling experiments, the structures of enzymes and compounds were prepared. The enzyme structures were protonated with Protonate3D[37] algorithm implemented in the molecular

modeling tool MOE.[38] The structures were energy minimized using Amber99 force field with all the heteroatoms and solvent molecules present in the protein. The backbone atoms were restrained with a small force in order to avoid collapse of the binding pockets during energy minimization calculations. After minimization, the co-crystallized ligands and solvent molecules were removed.

Compounds preparation. The 3D structural coordinates of the compounds were generated for all the compounds using MOE followed by assignment of protonation and ionization states in physiological pH range by using the "wash" module. Afterwards, the compounds' structures were energy minimized with the MMFF94x force field for the docking studies.

Docking studies. For the docking studies, AutoDock Tools[39] was used to add atomic partial charges. Newly synthesized triazolothiadiazole and triazolothiadiazine were docked into the active sites of AChE and BChE using the Lamarckian Genetic Algorithm in AutoDock 4.2. High-scoring docking poses were selected as putative binding modes for visual inspection. The Discover Studio 4.0 Visualizer was used for visualizing the results.[40] Drug likeness and oral bioavailability of studied compounds were evaluated using lipinski's violation filter.[41] Topological polar surface area (TPSA) of a molecule is defined as the surface sum of all polar atoms and shows the summation of polar fragments showing bonding patterns of a molecule.[42]

X-ray structure determination. Data for **4i** and **5e** were collected on an Oxford SuperNova CCD diffractometer using Mo-Kα ($\lambda = 0.71073$ Å) X-radiation at 130 K. The structures were solved by direct methods and refined by full-matrix least squares using SHELX-2014.

Acknowledgements

The authors would like to sincerely appreciate the Deanship of Scientific Research at King Saud University for its funding through the Research Group Project no RGV-VPP-345.

References

1 K. P. Kepp, *Chem. Rev.*, 2012, **112**, 5193–5239.
2 P. Faller and C. Hureau, *Chem.–Eur. J.*, 2012, **18**, 15910–15920.
3 T. Hartmann, J. Kuchenbecker and M. O. W. Grimm, *J. Neurochem.*, 2007, **103**, 159–170.
4 M. G. Savelieff, S. Lee, Y. Liu and M. H. Lim, *ACS Chem. Biol.*, 2013, **8**, 856–865.
5 M. Cygler, J. D. Schrag, J. L. Sussman, M. Harel, I. Silman, M. K. Gentry and B. P. Doctor, *Protein Sci.*, 1993, **2**, 366–382.
6 E. Giacobini, *Pharmacol. Res.*, 2004, **50**, 433–440.
7 E. Groner, Y. Ashani, D. Schorer-Apelbaum, J. Sterling, Y. Herzig and M. Weinstock, *Mol. Pharmacol.*, 2007, **71**, 1610–1617.
8 S. Y. Chiou, C. F. Huang, M. T. Hwang and G. Lin, *J. Biochem. Mol. Toxicol.*, 2009, **23**, 303–308.
9 J. L. Cummings, *N. Engl. J. Med.*, 2004, **351**, 56–67.
10 M. M. Mesulam, A. Guillozet, P. Shaw, A. Levey, E. G. Duysen and O. Lockridge, *Neuroscience*, 2002, **110**, 627–639.
11 (*a*) H. M. Greenblatt, H. Dvir, I. Silman and J. L. Sussman, *J. Mol. Neurosci.*, 2003, **20**, 369–383; (*b*) R. Cacabelos, *J. Mol. Biol.*, 2008, **448**, 213–357; (*c*) A. Contestabile, *Behav. Brain Res.*, 2011, **221**, 334–340.
12 M. B. H. Youdim, J. P. M. Finberg and K. F. Tipton, in *Monoamine Oxidase*, ed. U. Tredelenburg and N. Weiner, Springer-Verlag, Berlin, 1988, pp. 119–192.
13 K. N. Westlund, R. M. Denney, R. M. Rose and C. W. Abell, *Neuroscience*, 1988, **25**, 439–456.
14 A. S. Kalgutkar, D. K. Dalvie, N. Castagnoli and T. J. Taylor, *Chem. Res. Toxicol.*, 2001, **14**, 1139–1162.
15 T. P. Singer, in *Chemistry and Biochemistry of Flavoenzymes*, ed. F. Müller, CRC Press, Boca Ratón, FL, USA, 1990, vol. III, pp. 437–470.
16 (*a*) M. B. H. Youdim, D. Edmondson and K. F. Tipton, *Nat. Rev. Neurosci.*, 2006, **7**, 295–309; (*b*) M. Bortolato, K. Chen and J. C. Shih, *Adv. Drug Delivery Rev.*, 2008, **60**, 1527–1533.
17 (*a*) C. W. Muir, A. R. Kennedy, J. M. Redmond and A. J. B. Watson, *Org. Biomol. Chem.*, 2013, **11**, 3337–3340; (*b*) I. Khan, S. Ali, S. Hameed, N. H. Rama, M. T. Hussain, A. Wadood, R. Uddin, Z. Ul-Haq, A. Khan, S. Ali and M. I. Choudhary, *Eur. J. Med. Chem.*, 2010, **45**, 5200–5207; (*c*) I. Khan, M. Hanif, A. A. Khan, N. H. Rama, M. T. Hussain, M. A. S. Aslam and J. Iqbal, *Aust. J. Chem.*, 2012, **65**, 1413–1419; (*d*) I. Khan, A. Ibrar, M. Waqas and J. M. White, *Phys. Rev. Res. Int.*, 2013, **3**, 10–17; (*e*) A. Ibrar, I. Khan and N. Abbas, *Arch. Pharm. Chem. Life Sci.*, 2013, **346**, 423–446; (*f*) I. Khan, A. Ibrar and N. Abbas, *Arch. Pharm. Chem. Life Sci.*, 2014, **347**, 1–20; (*g*) M. Hanif, I. Khan, N. H. Rama, S. Noreen, M. I. Choudhary, P. G. Jones and M. Iqbal, *Med. Chem. Res.*, 2012, **21**, 3885–3896; (*h*) I. Khan, A. Ibrar, N. Abbas and A. Saeed, *Eur. J. Med. Chem.*, 2014, **76**, 193–244; (*i*) I. Khan, A. Ibrar, W. Ahmed and A. Saeed, *Eur. J. Med. Chem.*, 2015, **90**, 124–169.
18 S. N. Swamy, Basappa, B. S. Priya, B. Prabhuswamy, B. H. Doreswamy, J. S. Prasad and K. S. Rangappa, *Eur. J. Med. Chem.*, 2006, **41**, 531–538.
19 (*a*) B. S. Holla, K. N. Poojary, B. S. Rao and M. K. Shivananda, *Eur. J. Med. Chem.*, 2002, **37**, 511–517; (*b*) I. Khan, A. Ibrar and N. Abbas, *Eur. J. Med. Chem.*, 2013, **63**, 854–868.
20 J. T. Witkoaski, R. K. Robins, R. W. Sidwell and L. N. Simon, *J. Med. Chem.*, 1972, **15**, 150–154.
21 K. S. Bhat, B. Poojary, D. J. Prasad, P. Naik and B. S. Holla, *Eur. J. Med. Chem.*, 2009, **44**, 5066–5070.
22 R. Gupta, S. Paul, A. K. Gupta and P. L. Kachroo, *Indian J. Chem.*, 1994, **33B**, 888–891.
23 (*a*) V. Mathew, J. Keshavayya and V. P. Vaidya, *Eur. J. Med. Chem.*, 2006, **41**, 1048–1058; (*b*) V. Mathew, D. Giles, J. Keshavayya and V. P. Vaidya, *Arch. Pharm.*, 2009, **342**, 210–222; (*c*) P. Karegoudar, D. J. Prasad, M. Ashok, M. Mahalinga, B. Poojary and B. S. Holla, *Eur. J. Med. Chem.*, 2008, **43**, 808–815; (*d*) M. S. Karthikeyan, B. S. Holla, B. Kulkuraya and N. S. Kumari, *Monatsh. Chem.*, 2007, **138**, 1309–1316.
24 D. Sunil, A. M. Isloor, P. Shetty, K. Satyamoorthy and A. S. B. Prasad, *Arabian J. Chem.*, 2010, **3**, 211–217.

25 I. Khan, S. Hameed, N. A. Abdul-Reda, N. A. Al-Masoudi and J. Simpson, *Z. Naturforsch., B: Chem. Sci.*, 2015, **70**, 47–58.
26 (*a*) M. Hanif, M. Saleem, M. T. Hussain, N. H. Rama, S. Zaib, M. A. M. Aslam, P. G. Jones and J. Iqbal, *J. Braz. Chem. Soc.*, 2012, **23**, 854–860; (*b*) A. P. Skoumbourdis, C. A. LeClair, E. Stefan, A. G. Turjanski, W. Maguire, S. A. Titus, R. Huang, D. S. Auld, J. Inglese, C. P. Austin, S. W. Michnick, M. Xia and C. J. Thomas, *Bioorg. Med. Chem. Lett.*, 2009, **19**, 3686–3692.
27 D. Lauffer, P. Li and K. Mcginty, EP 2 435 443 B1, July 31, 2013.
28 I. Khan, S. Zaib, A. Ibrar, N. H. Rama, J. Simpson and J. Iqbal, *Eur. J. Med. Chem.*, 2014, **78**, 167–177.
29 I. Khan, A. Ibrar, S. Zaib, S. Ahmad, N. Furtmann, S. Hameed, J. Simpson, J. Bajorath and J. Iqbal, *Bioorg. Med. Chem.*, 2014, **22**, 6163–6173.
30 S. M. I. Badr and R. M. Barwa, *Bioorg. Med. Chem.*, 2011, **19**, 4506–4512.
31 F. H. Allen, *Acta Crystallogr.*, 2002, **B58**, 380–388.
32 P. Politzer, J. S. Murray and T. Clark, *Phys. Chem. Chem. Phys.*, 2013, **15**, 11178–11189.
33 G. L. Ellman, K. D. Courtney, V. Andres Jr and R. M. Feather-Stone, *Biochem. Pharmacol.*, 1961, **7**, 88–95.
34 A. Stössel, M. Schlenk, S. Hinz, P. Küppers, J. Heer, M. Gütschow and C. E. Müller, *J. Med. Chem.*, 2013, **56**(11), 4580–4596.
35 S. A. Hitchcock and L. D. pennington, *J. Med. Chem.*, 2006, **49**(26), 7559–7583.
36 D. S. Goodsell, *Computational docking of biomolecular complexes with AutoDock*, Cold Spring Harb Protoc, 2009, pdb prot5200.
37 P. D.h.w.c.c.j.p.h. P. Labute, http://www.chemcomp.com/journal/proton.htm.
38 C.C.G.I.h.w.c.c. MOE (The Molecular Operating Environment) Version 2010.10. Chemical Computing Group Inc, http://www.chemcomp.com.
39 G. M. Morris, R. Huey, W. Lindstrom, M. F. Sanner, R. K. Belew, D. S. Goodsell and A. J. Olson, *J. Comput. Chem.*, 2009, **30**, 2785–2791.
40 Accelrys Software Inc., *Discovery Studio Modeling Environment, Release 4.0*, Accelrys Software Inc., San Diego, CA; 2013.
41 V. N. Wouatsa, L. Misra, S. Kumar, O. Prakash, F. Khan, F. Tchoumbougnang and R. K. Venkatesh, *Chem. Cent. J.*, 2013, **7**, 125–139.
42 P. Ertl, B. Rohde and P. Selzer, *J. Med. Chem.*, 2000, **43**, 3714–3717.